



Shape Memory Materials Analysis and Research Tool (SM²ART): Finding Data Anomalies and Trends

P. E. Caltagirone^{1,2} · O. Benafan¹

Received: 22 February 2023 / Revised: 30 June 2023 / Accepted: 6 July 2023
© ASM International 2023

Abstract Typically, the first step in alloy selection and material production is to use handbooks, databases, or other materials guides to down-select to a specific composition and processing method for the desired application. This is true for conventional materials, such as steels, aluminums, and polymers, but until recently, no similar data source existed for shape memory materials (SMMs). There is no shortage of information in the SMM field; with over 90 years of research in the form of peer-reviewed articles, papers, and published data from companies; however, these data have not been accessible in a single location. This has posed many difficulties for the research and development of SMMs and has caused the field to move slowly. To remedy this, a web-based comprehensive repository known as the Shape Memory Materials Analysis and Research Tool (SM²ART) database has been developed. SM²ART provides unrestricted access to data from thousands of peer-reviewed articles and published data. These data are organized in a 2D and 3D visualization platform and provides viewers insight into shape memory alloys (SMAs), superelastic alloys, magnetic alloys, shape memory polymers (SMPs), and shape memory ceramics (SMCs). The work presented here provides a summary of the data available within the SM²ART database.

Keywords Shape memory materials · Database · SMA · Shape memory ceramics · Shape memory polymers · Magnetic shape memory · Superelasticity

Introduction

Shape memory materials (SMMs) have been of high interest in the scientific community since the shape memory phenomenon was first observed in AuCd in the 1930s. The discovery and relative stability of NiTi shape memory alloys (SMAs) in the 1950s led to the adaptation of these materials for use in applications beyond scientific research. The biomedical industry has maintained a strong interest due to these alloys' ability to demonstrate a superelastic (SE) effect with high reversible strains (up to 6% in most common SMAs), which is especially useful for medical applications such as stents, orthodontic wires, and other devices. In addition to superelasticity, SMAs also exhibit the shape memory effect (SME), in which a deformed material can undergo a diffusionless transformation under a thermal load and revert back to its original shape. This phenomenon has driven increased interest within the aerospace and automotive industries for potential uses of SMAs as lightweight, thermally activated actuators capable of reducing the footprint and weight of existing systems and facilitating new designs. Along with SMAs' unique and advantageous properties also come many complexities that have hindered commercial interest in the materials, slowing their introduction into the general market. High processability dependence, manufacturing, qualification, and chemical sensitivity are some of the challenges being addressed to improve market traction. These issues are not unique to SMAs; other SMMs, such as shape memory

✉ P. E. Caltagirone
peter.e.caltagirone@nasa.gov

¹ Materials and Structures Division, NASA Glenn Research Center, Cleveland, OH 44135, USA

² Materials and Structures Division, NASA Glenn Research Center, Oak Ridge Associated Universities, Cleveland, OH 44135, USA

polymers (SMPs) and shape memory ceramics (SMCs), exhibit similar shape memory and superelastic phenomena.

Table 1 lists various types of SMMs that exhibit superelastic and shape memory behavior, or some comparable effect. SMAs, the most studied SMMs, are comprised of many alloy bases, from the conventional NiTi-based to the lesser-known U-based systems. Magnetic or ferromagnetic SMAs have also surged in popularity as potential materials for actuator applications due to the fast-switching rates of NiMn-based and FePd-based alloys, among others. SMPs exist in over 85 chemical families and can be triggered by stress, heat, sunlight, or solvents. Some of these polymers are actively being used in products in the biomedical field. In the SMC category, compositions such as ZrO₂ could lead to new applications in microelectronics, flow devices, heat mitigation, and other fields. Studies have combined one or more of these SMMs to form composites, which are capable of exhibiting unique features.

The plethora of SMM options provides an unparalleled resource for the design of new materials and components, but access to such collective information has been very limited. For traditional materials such as steels and aluminums, handbooks and databases are used as guidelines for forming and processing known alloys, and provide a solid foundation for designing new materials or processes. These handbooks and databases also contain valuable information on the physical, chemical, and mechanical

capabilities of each alloy. In addition to materials handbooks and databases, a myriad of standards provides guidelines for testing and qualifying traditional materials. Similar guidance for SMMs, however, has been sparse to nonexistent, often available only in the form of peer-reviewed articles scattered throughout journals or via testing results published by companies. Researchers face challenges finding and comparing data, identifying gaps in research, and avoiding possible duplication of research. Furthermore, without a single source of data, the possibility of data informatics or machine learning has been very limited.

To remedy this issue, limited shape memory databases have been developed in an attempt to facilitate growth and provide a common space for the data. Although all of these databases provide data on SMMs, most are very limited in the data, the pedigree, and the tools provided for analysis of the data. The lack of a single data source and analysis tools led to the creation of the Shape Memory Materials Analysis and Research Tool (SM²ART) database presented in this work. Table 2 provides an overview of legacy and current SMM handbooks and databases, including the SM²ART database.

The SM²ART database provides one-stop access to SMM data, including SMAs, superelastic alloys, magnetic shape memory alloys (MSMAs), SMPs, and SMCs [56, 57]. The data are organized in a 2D and 3D

Table 1 Shape memory materials categories and their common formulations

Category	Acronym/ abbreviation	Example formulations	Potential application examples
Shape memory alloys	SMAs	Ag-based, Au-based, Cu-based, In-based, Mg-based, NiAl-based, NiTi-based, Pd-based, Ru-based,	Medical (NiTi-based) [1–16], aerospace (NiTi-based, Cu-based) [17–20], optics (NiTiPd-based) [21, 22], nuclear system (U-based) [23, 24]
Superelastic	SE	Ti-based, U-based, Zr-based	
Magnetic shape memory alloys	MSMAs	Fe-based, NiMn-based	Energy harvesting [25–27]
Shape memory polymers	SMPs	Cellulose, EPDM, epoxy resin, nitrile rubber, poly-based (PTFE, polyacrylamide, poly(amide-co-ether), polyacrylate, polyester, polyimide, PMMA, etc.), silicone, styrene butadiene rubber	Clot removal devices [28, 29], vascular stents [30, 31], orthodontic appliances [32, 33], auto-constricting sutures [34], dialysis needles [35], thermally induced constricting or loosening fabrics, wrinkle-free fabrics, impact-resistant fabrics [36–40], deployable solar arrays, truss systems, antennas, morphing structures [41–48]
Shape memory ceramics	SMCs	BT, BFO, NBT, PLZST, PLZT, PMN(Pb), PNZST, ZrO ₂ -based (Ca, Ce, Dy, Gd, Hf, Mg, Ti, Y, Yb)	Fast-actuation latching relay device [49]
Composites	Comp	Epoxy resin-SMA wire, polymer-polymer	Medical devices, acoustic failure detection, strengthened adhesive bonds with SMA wire entanglement, [50–52]

This table is not inclusive of all materials systems, and other formulations may exist

Table 2 Legacy and current shape memory materials databases and handbooks

Name	Source	Contact	Overview	Ref.
SMA-Select	https://hal.archives-ouvertes.fr/jpa-00250565/document	J. phys., IV (W. Tang et al.)	No online availability. Binary NiTi data pre-1991 is presented with SMA and SE experimental data	[53]
Smart Materials Database	https://rsmith.math.ncsu.edu/Smart_Materials_Database/	NC State University (R. Smith et al.)	Open-source data for ferroelectric actuators and binary NiTi SMAs. Computational tools available for analysis of experimental data	[54]
ASM Handbook	ASM Handbook, Vol. 2: pp. 897–902 DOI: https://doi.org/10.31399/asm.hb.v02.a0001100	ASM International (D. Hodgson et al.)	Membership: Provides some historical background on SMAs along with their properties	[55]
Shape Memory Materials Analysis and Research Tool (SM ² ART) Database	https://shapememory.grc.nasa.gov/	NASA (O. Benafan et al.)	Open-source database containing over one and a half a million data points and pedigree for SMAs, superelastic alloys, magnetic alloys, SMPs, and SMCs. All data and trends can be plotted and analyzed	[56, 57]

visualization platform that allows users to plot any of the available data to a figure for any of the available systems. Users can plot using multiple tools, including scatter, box-and-whisker, and sun plots as well as ternary diagrams. Additional basic analysis tools are available, including clustering and regression for simple investigation of the material systems. This framework also offers an approach to upload custom data (experimental or computational), which can be visualized and analyzed alongside the available data during an active session (custom data is not saved).

This work provides an overview of the SM²ART database and the capabilities available for unrestricted public use within the database. A description of the data and tools available in SM²ART is provided below, followed by a brief review of each SMA base alloy in the database. Following this, a brief review of MSMAs, SMPs, and SMCs is given.

Database Data and Tools

The information presented in the SM²ART database is a collection of data and metadata extracted from 1000 of peer-reviewed published articles and other sources [56]. Data collection was performed in an unbiased manner to include all data from a given source, and users are able to filter data at their discretion. The data have been processed and reviewed to remove data extraction errors, create common terminology, and add valuable information, such as calculated density and estimated cost.

Figure 1 shows the path of the SMM data from collection through categorization and into the database tool. In its

current format, the SM²ART database contains experimental data from peer-reviewed references, proceedings, and dissertations and allows users to upload and view custom experimental or modeled data within a working session. Once a relevant reference is identified, the article is reviewed and the data are collected from the document and sorted by a number of parameters (material type, formulation, processing, test type, test direction, etc.) to ensure the metadata in reported values, such as transformation temperatures, can be accurately captured and explained. Once collected, data are imported internally into the online database, allowing users access to 2D and 3D data in the form of scatter plots, box-and-whisker plots, and ternary diagrams while also providing valuable tools such as unsupervised machine learning (e.g., k-means clustering) and polynomial regressions. Supervised machine learning algorithms that take advantage of this large dataset have been formulated [58] and are currently being implemented as one of the latest SM²ART database tool sets. Custom data uploads are not currently captured and stored in the SM²ART database; these data can only be utilized while the user is an active session. Uploading and saving data to the database follow a different path to ensure data traceability, and this feature is the subject of future releases.

Recognizing the need for data customizability depending on the end user (e.g., researcher, designer, or modeler), the SM²ART database was built with a number of useful features to intuitively help the exploration process and focus on user priorities. This includes customized interfaces to select chemistries based on materials type, custom plotting and axes control, data and property filters, and multi-system and multi-element selection options. This

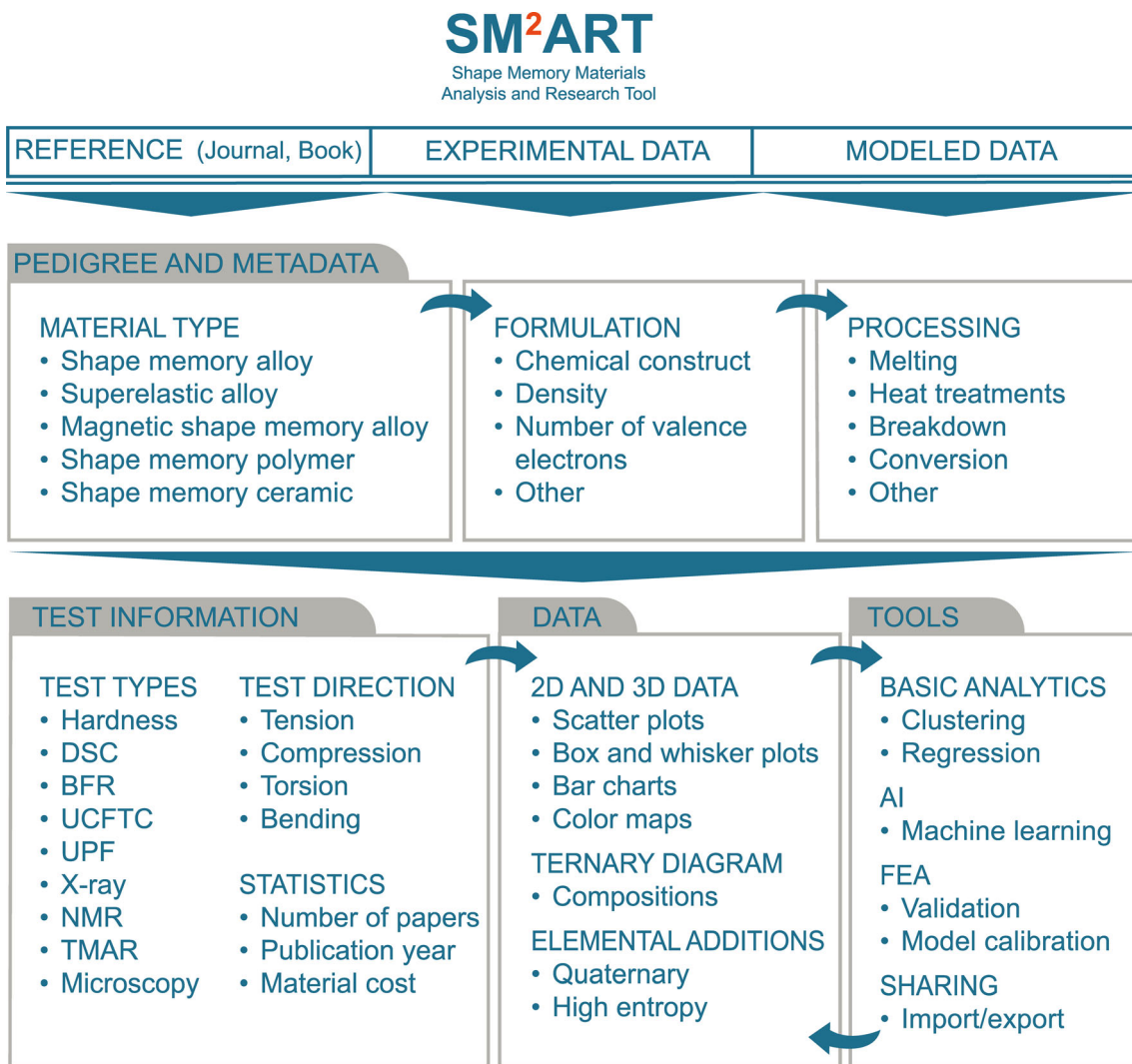


Fig. 1 Data extraction process and tools for SM²ART database

setup is applied to all five material types (SMAs, superelastic materials, MSMAs, SMPs, and SMCs), which can be accessed via a material type selection tab. As of this publication, the SM²ART database contains the following number of experimental data records (with additional entries continuously being added):

- 611,644 independent data records from the shape memory alloy category
- 35,461 independent data records from the superelastic alloy category
- 61,340 independent data records from the magnetic alloy category
- 793,450 independent data records from the shape memory polymer category
- 30,850 independent data records from the shape memory ceramics category

Each of these data records is fully traceable from each datapoint plotted within the SM²ART database. Table 3 compares SM²ART database capabilities with the SMA-SELECT [53] database and the Smart Materials Database [54].

Figure 2 provides a snapshot of the SM²ART database capabilities for visualization and analysis of data. The SM²ART database allows users to plot data directly within the application, a capability not present in most of the current SMM databases. Viewing this data in a graphical format can easily reveal trends that would otherwise be difficult to determine. In addition to plotting, it is possible to use data filters within the SM²ART database to further screen the data. If users are seeking data on specific processing methods, heat treatments, compositions, etc., it takes only a few clicks to reveal the filtered data set, a feature unavailable in other SMM databases. Once the data are plotted, the SM²ART database provides users with a

Table 3 SM²ART database capabilities comparison

	Open access	Comp. data	Exp. data	Data upload	Web API	Data analysis tools	Material type	Data records
SMA-SELECT [53]	✓ ^a		✓				1, 2	10 ²
Smart Materials Database [54]	✓		✓		✓	✓ ^b	1, 2	10 ³
SM ² ART Database [this work]	✓	✓	✓	✓ ^c	✓	✓	1 to 5	> 10 ⁶

Open access: provides free access to available data. Computational data (*Comp. Data*): data collected from computational simulations. Experimental data (*Exp. Data*): data collected from lab experiments. Data upload: allows users to upload custom data to the database. Website application programming interface (*Web API*): available remotely via a publicly open website

^aPublished article available with limited data

^bMATLAB-based data tools available for download

^cCustom data only viewable during active user session; not saved

1 = SMAs, 2 = SE alloys, 3 = MSMAs, 4 = SMPs, 5 = SMCs

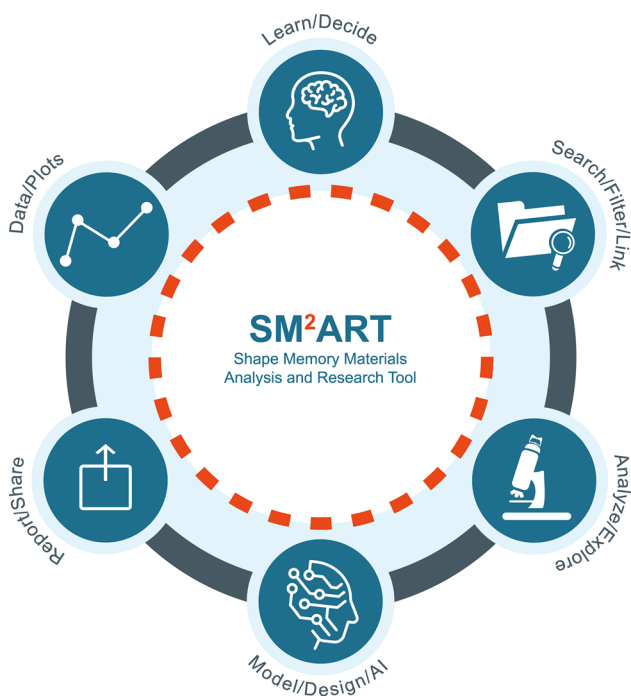


Fig. 2 SM²ART database capabilities for data access, visualization, and analysis

number of analysis tools, such as regression and k-means clustering, to assist in discovering trends within the data. The ability to quickly export an image file allows users to easily report and share any of the data, which can be used to learn about new alloys and decide the best course of action when designing for a new material or application.

Overview of Shape Memory Alloy Systems

Although NiTi-based alloys are the most commonly studied SMA types, many other alloy systems offer unique attributes and may be better suited for a given application. One of the SM²ART database's objectives is to bring forth a collection of SMA systems in order to explore them individually or in tandem with each other. There are currently 15 distinct SMA base alloy systems available for viewing and exploration: Ag, AuCd, AuCu, AuZn, CuAl, In, Mg, NiAl, NiTa, NiTi, Pd, Ru, Ti, U, and Zr. (Other systems may exist, but they are not currently within the SM²ART database arsenal.) The characteristics of each SMA depend upon a number of variables in the synthesizing and processing of the material; these variables govern the subsequent properties of the material. Such variables include elemental composition, melting practice, processing method, and heat treatment temperature and time, among others. Most of these variables are documented as pedigree data and are accessible within the SM²ART database framework. When collectively compared, the similarities or differences in properties within each material system are accentuated, thus opening up new material design opportunities that might otherwise be left unexplored. As an example, Fig. 3 compares the hysteresis width and austenite finish (A_f) temperatures of all SMA systems available in the SM²ART database. It is noted that the AuZn- and Mg-based systems currently have insufficient data of this type to be included in the figure.

A side-by-side comparison of technical data, as exemplified in Fig. 3, offers many useful insights into material capabilities. When considering A_f temperatures, the data indicate that Ag-based alloys have the lowest A_f temperatures and Ti-based alloys have the highest available A_f temperatures; however, the NiTa-based system has the

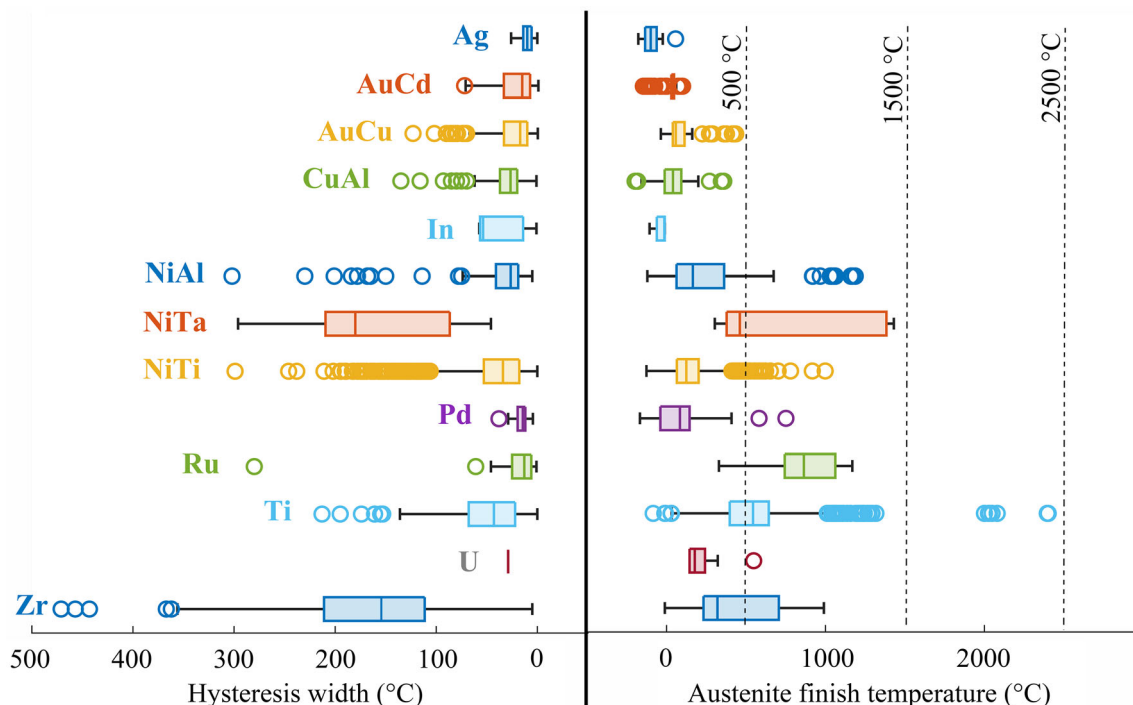


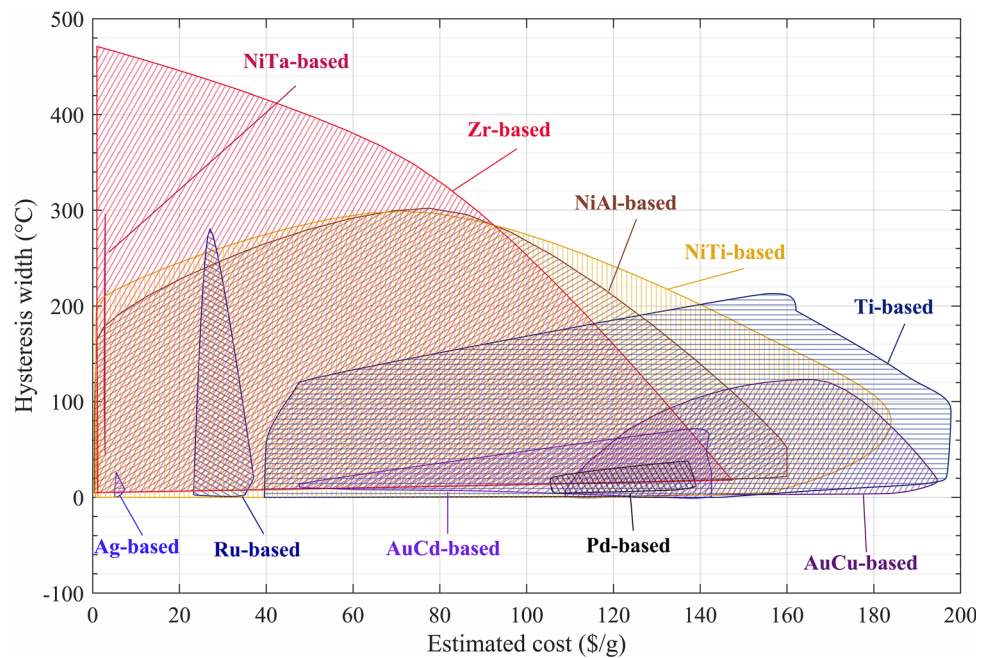
Fig. 3 Hysteresis width and austenite finish temperature ranges for SMA base systems available in the SM²ART database

highest transformation temperatures that are not considered outliers. As for the hysteresis width, the data indicate that while most systems are capable of low hysteresis, the Ag and Pd-based systems are the most consistent.

When cost is a consideration, such information can be cross-referenced among the different alloy systems, as shown in Fig. 4. Ag- and Pd- systems show the lowest

hysteresis but have very different base material costs; Ag-based alloys can be acquired for $\sim \$7/g$ to $\$10/g$, whereas Pd-based alloys range from $\sim \$105$ to $\$140/g$ (based on 2022 prices). These cost estimates take into consideration only the cost of the raw materials; material processing and manufacturing costs can add significantly to final product costs.

Fig. 4 Hysteresis width plotted against estimated cost in US dollars per gram for various SMA systems (prices captured February 2022). Systems with insufficient data are not displayed. Data clusters envelop all edge data points within the SM²ART database



Further down-selection can be performed to refine the search. As some material bases are eliminated from the current exploration, tertiary or higher search criteria can be applied as shown in Fig. 5. Initially, it may seem that Ag-based systems are the only materials to consider for low hysteresis due to their considerably lower material cost. This does not consider all variables, however, such as material strength. According to Fig. 5, Pd-based SMAs are capable of nearly double the strength of Ag-based alloys, which may be crucial for successful implementation of an SMA in a given application. An approach that compares multiple layers of the same dataset will ultimately lead to an optimal design within the confines of the available datasets.

When designing systems incorporating SMAs (e.g., actuators and elastocaloric devices), the martensite finish (M_f) and A_f temperatures are critical parameters, as they dictate the operating bounds of the design process. Figure 6 shows M_f and A_f temperatures for all SMA data currently available in the SM²ART database, represented as an envelope of the scatter data. Figure 6a includes systems capable of low to medium temperature transformation (less than 500 °C), whereas Fig. 6b shows systems capable of medium to high temperature transformation (greater than 500 °C). This plot provides a very useful overview of SMA capabilities, which may be beneficial in selecting a specific system for further examination. Each individual alloy system can be subdivided into alloying groups to better understand how the base alloy composition affects transformation temperatures. For example, the NiTi-based alloy system includes 35 distinct ternary alloying additions,

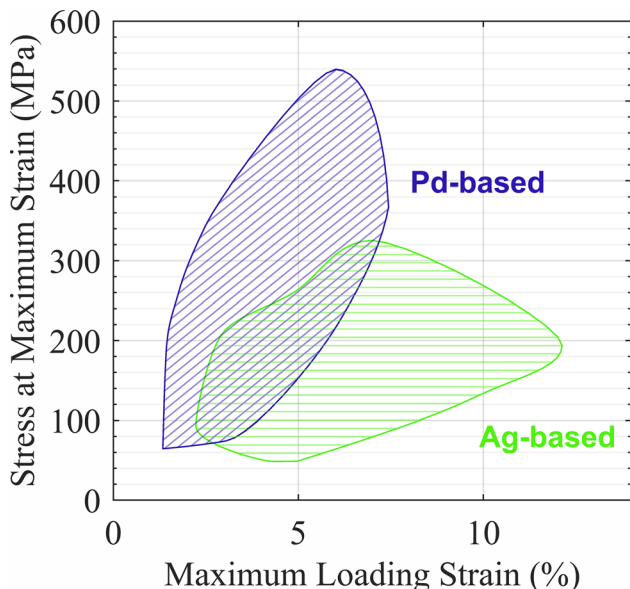


Fig. 5 Comparison of maximum stress as a function of maximum loading strain for Ag-based and Pd-based systems in the SM²ART database

many quaternary formulations, and a relatively smaller number of quinary or higher-order elemental aggregates. Each alloying group serves to achieve a specific property, such as transformation temperatures. Such plots can be constructed for any properties available within the SM²ART database (e.g., actuation strain, applied stress, valence electrons, and density).

Figures 7, 8, and 9 provide more in-depth transformation temperature information for each material system. Figure 7a shows the A_f versus M_f transformation temperatures for Ag-based alloys, with A_f temperatures ranging from –180 °C to approximately –20 °C. Other Ag-based alloys also exist beside AgCd within the SM²ART database (AgAl and AgZn), but they are not displayed in this chart due to lack of data for A_f , M_f , or both. Figure 7b demonstrates the AuCd-based alloys with three different subsystems: the binary AuCd alloys and the ternary AuCdCu and AuCdAg alloys. The binary alloys have A_f temperatures ranging from around 25 to 100 °C. The addition of Cu is shown to lower transformation temperatures to a range of –45 to 50 °C, whereas the addition of Ag to binary AuCd lowers transformation temperatures to a range of –150 to –10 °C. Figure 7c shows the AuCu alloy and its subsystems within the available data. AuCuAl has a temperature range of 0 to 380 °C. The addition of Zn to AuCu results in temperatures ranging from –40 up to approximately 280 °C. Within the AuCu system, limited data for quaternary alloys are available. AuCuAlFe is shown with an A_f around 15 °C. Figure 7d shows transformation temperatures for the CuAl-based alloys. To date, only CuAlMn data are available; other CuAl alloys will be catalogued in future work. The CuAlMn A_f varies from –200 °C to 340 °C, whereas the CuAlMnFe system has limited data in the –20 °C to 40 °C range. Figure 7e and f shows transformation temperatures for the NiAl-based alloys. The most notable transformation temperature ranges are found in binary NiAl alloys, with an A_f range of 0 to 325 °C, and NiAlPt alloys, with a temperature range of 125 to 1200 °C.

Figure 8 encompasses the entirety of the NiTi-based alloy system, showing the available A_f and M_f transformation temperatures for the binary, ternary, quaternary, and quinary elemental additions—59 distinct alloys in all. These alloys are capable of a wide range of temperatures, with some alloys reaching A_f temperatures as low as –100 °C (e.g., NiTiFe and NiTiSc) and as high as 1000 °C (NiTiPt). The elemental additions are not the only factor contributing to observed changes in temperatures; other aspects, such as base material percentage ratios, heat treatments, and cold/hot working, can have a large effect as well. The SM²ART database makes it possible for researchers to construct and use such information for more precise alloying and processing studies.

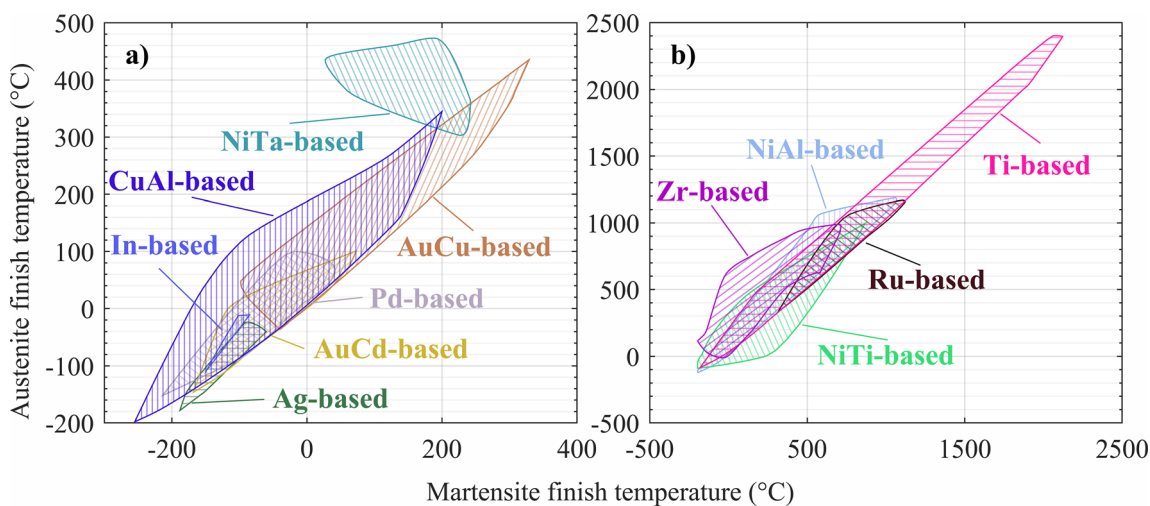


Fig. 6 Austenite finish temperature as a function of martensite finish temperature for SMA systems available in the SM²ART database repository. Systems with insufficient data of this type are not displayed. Axis limits are uniquely displayed to better visualize the data trends

Figure 9 shows the remaining systems with available transformation temperature data in the SM²ART database. Figure 9a shows the NiTa-based alloys, with A_f temperatures ranging from roughly 300 to 470 °C for binary NiTa and limited data around 360 °C for NiTaB. Figure 9b shows the available data for the Pd-based alloys, with the PdMnSn system A_f temperatures ranging from –150 to –40 °C. The PdInFe alloys range from –10 to 100 °C. Figure 9c includes data from the Ru-based system. RuTa A_f temperatures range from 325 to 1175 °C, and RuNb temperatures range from approximately 325 to 1075 °C. Figure 9d shows the data for Zr-based alloys. The systems of most note are ZrCuNi and ZrCoNi, with A_f temperatures ranging from 180 to 850 °C and from 125 to 950 °C, respectively. Figure 9e and f show A_f temperatures for Ti-based alloys, with the lowest temperatures from the TiPdMn alloys, ranging from –10 to 175 °C, and the highest temperatures from the TiRhSc alloys, ranging from 2000 to 2400 °C.

Because each alloy system has different base elements, each with varying additional alloying elements, many different properties are possible within each system. Table 4 shows the capabilities of each material system for a given application type, such as actuators, superelastics, medical, magnetics, or elastocalorics. It should come as no surprise that the NiTi system is so widely used; the system is capable of all of the metrics listed, depending on the specific alloy composition used (Figs. 10, 11, 12, 13, 14, 15 and 16).

The following sections provide a brief overview of each alloy system, with additional details regarding the strengths and the various capabilities for which each system is known. The highlights provided in these sections also emphasize the importance of having all SMM data

available in a single source; the strengths and weaknesses of each system vary greatly and picking an alloy (or even other material) is a burdensome task without the benefit of a single source of data.

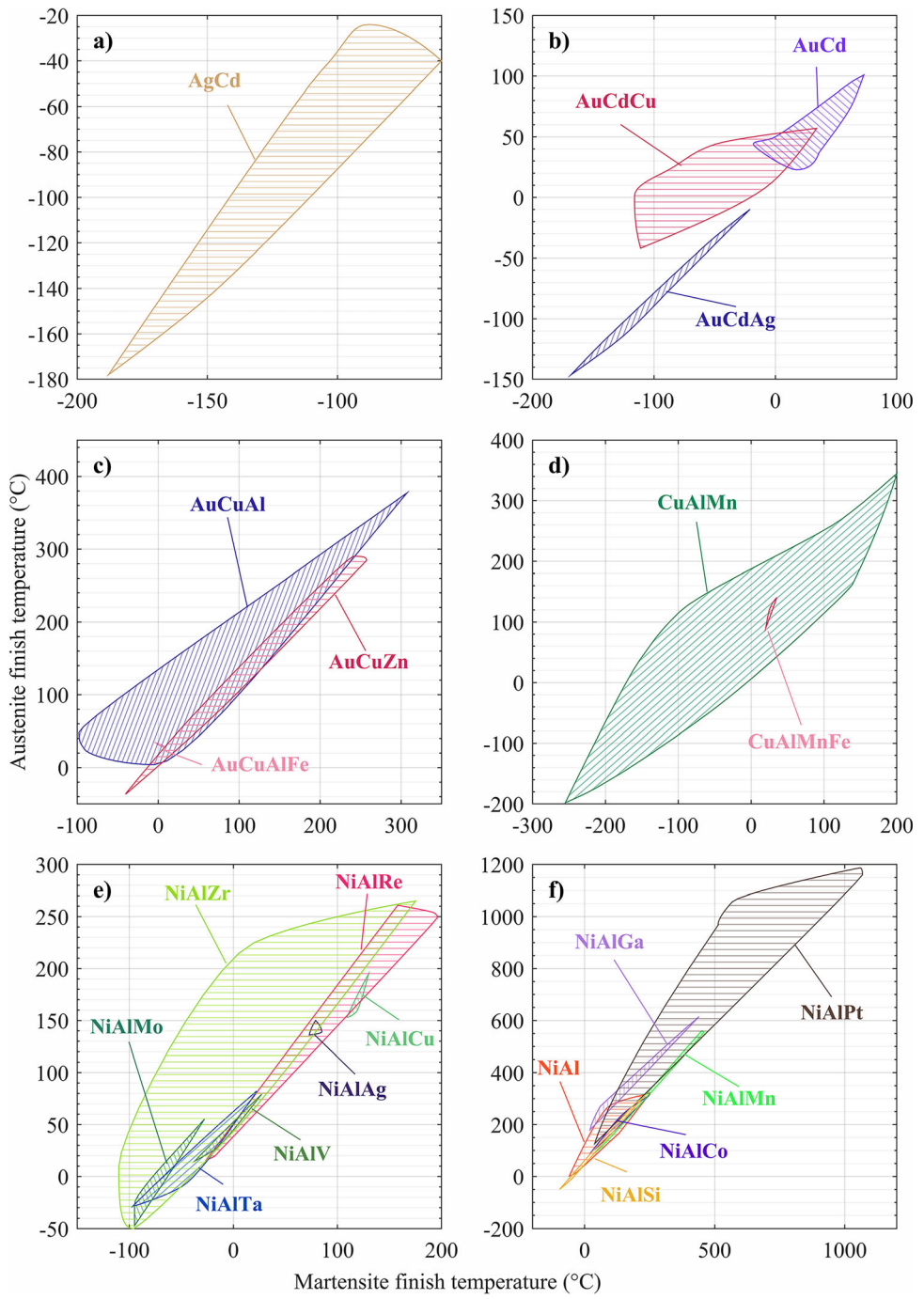
Ag-Based Alloys

Ag-based alloys that exhibit the SME have many beneficial properties; first and foremost is their transformation at low temperatures. With A_f temperatures ranging from –180 to 20 °C [59–66], these alloys may be suitable for low-temperature applications such as deep space exploration. These Ag-based alloys have also been shown to exhibit exceptionally low hysteresis (as low as 2 °C) [59, 62, 64, 65], a property often sought after in actuator applications. The Ag-based alloys have good workability and are nonferrous, lightweight, corrosion resistant, and non-magnetic, making them leading candidates for the electronic device market. As with most alloys, there are limitations on where these alloys can be used. The high cost of Ag, particularly for large-scale production, can be a deterrent to wider use, as can the low tensile strength exhibited by some of these alloys.

AuCd-Based, AuCu-Based, and AuZn-Based Alloys

In 1932, AuCd was the first alloy discovered to exhibit the SME [67]. AuCd alloys are capable of transformation temperatures ranging from –150 to 100 °C and are known to exhibit two different martensitic transformations, dependent on the AuCd composition and the aging process. Alloy compositions of Au_{52.5}Cd_{47.5} (at.%) undergo a β_2 (B2) to γ'_2 (orthorhombic) phase transformation, whereas alloy compositions closer to equiatomic undergo a β_2 (B2)

Fig. 7 A_f and M_f transformation temperatures for **a** Ag-based, **b** AuCd-based, **c** AuCu-based, **d** CuAl-based, and **e** and **f** NiAl-based alloys. Axis limits are uniquely displayed to better visualize the data trends

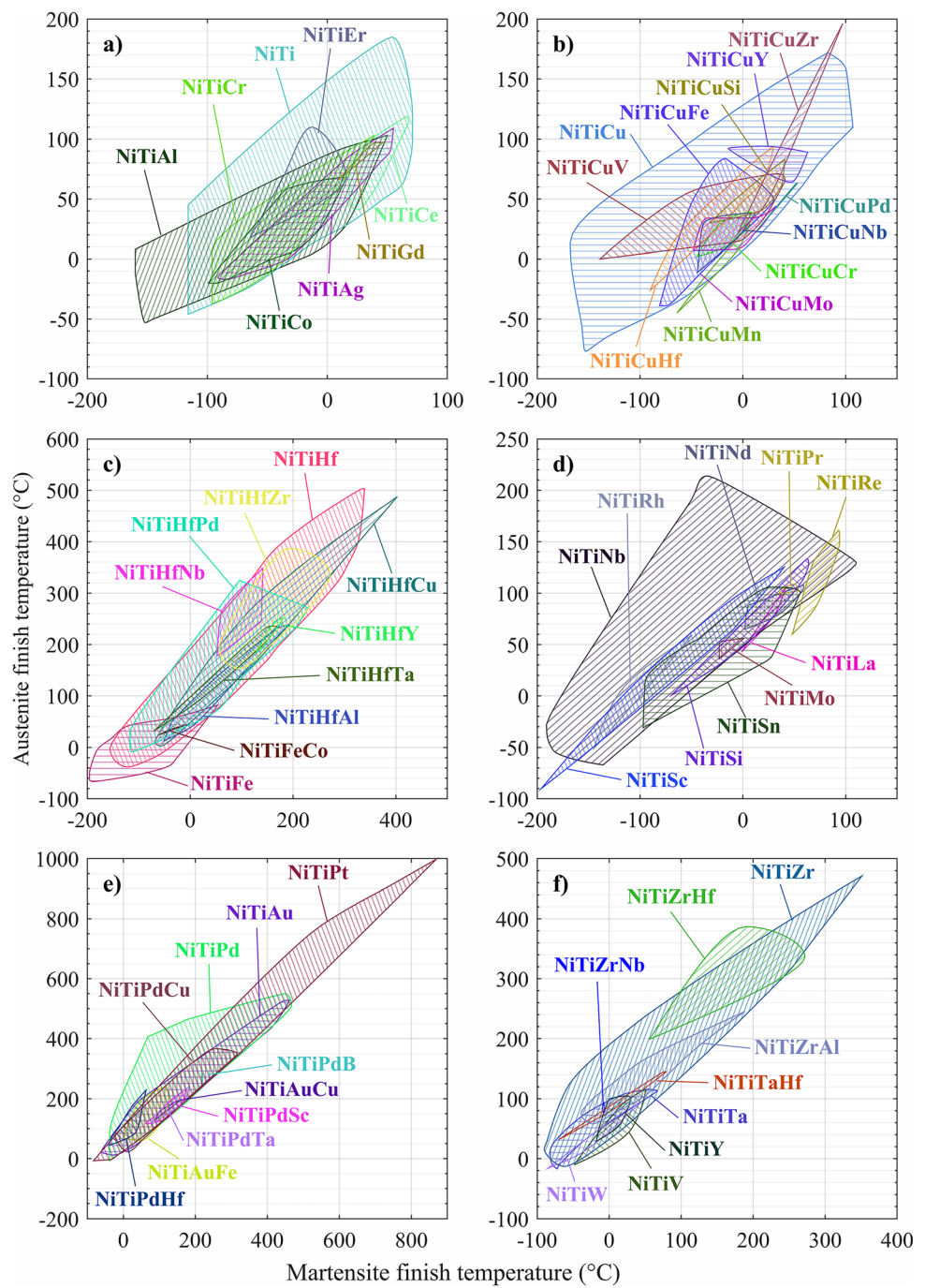


to ζ'_2 (trigonal) phase transformation [68–74]. Depending on this transformation path, AuCd with compositions near equiatomic exhibit a rubber-like behavior (RLB) in which after being aged in the martensite phase, the material demonstrates recoverable pseudoelastic deformation behavior in the martensite state [71–76]. Depending on the aging conditions, martensitic aging can also induce a stabilization effect in which the martensite phase becomes more stable, which is manifested by the increase in A_f

temperature. The A_f temperature is further elevated by increasing the aging time [69, 73, 74, 77].

Equiatomic AuCu alloys are known to exhibit two order-disorder transformations. The first transformation is from an $L1_0$ (tetragonal) structure to a pseudo-orthorhombic lattice, which occurs around 385 °C. The material then further transforms around 420 °C to an A1 [disordered face-centered cubic (FCC)] structure [78–86]. AuCu alloys may be good candidates for biomedical applications as they have good corrosion resistance,

Fig. 8 A_f and M_f transformation temperatures for NiTi-based alloys. Axis limits are uniquely displayed to better visualize the data trends



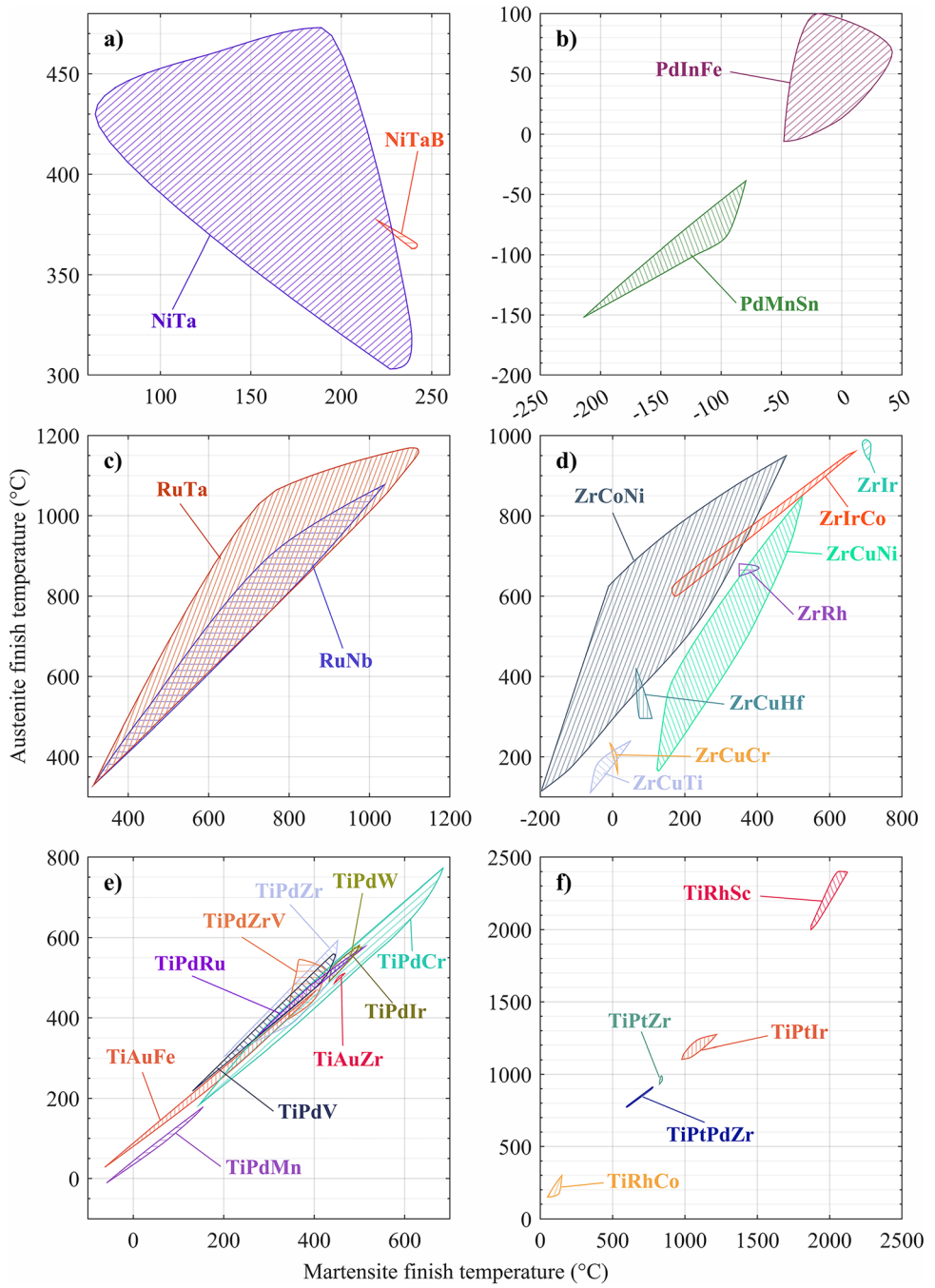
radiopacity, and mechanical performance. These alloys are already used for dentistry, electronics, and jewelry.

AuZn alloys are unique in that they exhibit very low transformation temperatures. These alloys have been reported to transform around -200 °C, with transformation temperatures ranging as low as -230 °C at a Zn content of 48 at.% up to -180 °C at a Zn content of 53 at.% [87–92]. These alloys may be very useful in cryogenic applications, where superelasticity is desired.

CuAl-Based and In-Based Alloys

CuAl alloys are of high interest in the SMA community for a number of reasons. The addition of Al raises the martensite start transformation temperature to roughly 200 °C [93–95], which is useful when higher transformation temperatures are required. Cu alloys are nonferrous and, in general, have high strength and elasticity, excellent wear, and corrosion resistance, making them excellent candidates for radiation shielding, step soldering, and

Fig. 9 A_f and M_f transformation temperatures for **a** NiTa-based, **b** Pd-based, **c** Ru-based, **d** Zr-based, and **e** and **f** Ti-based alloys. Axis limits are uniquely displayed to better visualize the data trends



more. The SME is observed in CuAl alloys et al. compositions between ~ 20 and 30 at.%, which transforms from β' to β or γ' to β structure depending on aluminum content [93–111]. The β and β_1 martensite phases can decompose into α and γ_1 phases after quenching, thus CuAl alloys are typically paired with an additional element (such as Mn) to stabilize the β and β_1 phases [94]. It is known that CuAl-based alloys are fracture prone in the polycrystalline aggregates, but the stabilization improvements in the

single-crystal forms are significant. Single-crystal CuAl-based alloys are used extensively in the space industry.

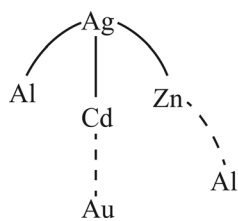
Pure indium has a stable face-centered tetragonal (FCT) structure. When combined with other elements such as Cd, Pb, or Tl at compositions ranging from 6 to 30 at.%, the material can exhibit a low-temperature SME (< 0 °C). In-Tl, In-Cd, and In-Pb alloys undergo a (FCC) to face-centered tetragonal (FCT) transformation upon heating [112–119]. The relatively low energy required for transformation from FCC to FCT (compared to other

Table 4 Possible application capabilities of the 15 SMA systems

	Actuator applications	Superelastic applications	Medical applications	Magnetic applications	Elastocaloric applications
Ag-based alloys	✓	✓	✓		
AuCd-based alloys	✓	✓			
AuCu-based alloys	✓	✓	✓		
AuZn-based alloys	✓	✓			
CuAl-based alloys	✓	✓			✓
In-based alloys	✓				
Mg-based alloys		✓			
NiAl-based alloys		✓		✓	
NiTa-based alloys		✓			
NiTi-based alloys	✓	✓	✓	✓	✓
Pd-based alloys	✓	✓	✓		
Ru-based alloys					
Ti-based alloys		✓		✓	
U-based alloys	✓				
Zr-based alloys		✓			

Actuator applications include shape recovery, constrained recovery, force generation, acoustics, sensing, etc. Superelastic applications include medical, tribology components, damping, corrosion, structural, etc. Elastocaloric applications include energy harvesting, thermal management systems, air conditioning, radiators, etc.

Fig. 10 Ag-based alloy and elemental aggregates. Dashed lines indicate higher-order alloying elements



liquid-crystal displays (LCDs), liquid emitting diodes (LEDs) and semiconductors; however, none of the alloys used for these applications exhibit a SME. One promising application for indium alloys is the use of manufactured indium nanowires in nanotechnology [119].

Mg-Based Alloys

Mg-based alloys are relatively new to the SMA field and have sparked much interest due to their high specific strength and lightweight characteristics [120–124]. On its

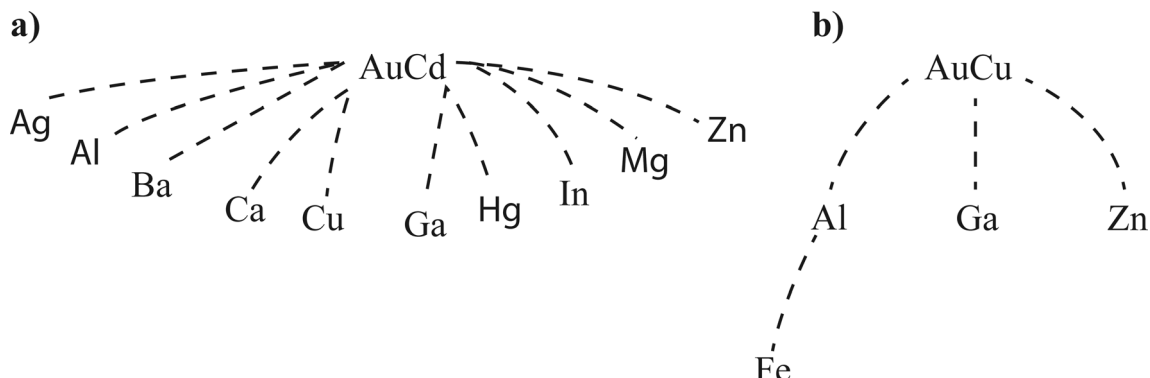


Fig. 11 **a** AuCd-based and **b** AuCu-based alloys and elemental aggregates. Dashed lines indicate possible higher-order alloying elements. AuZn alloys do not have higher-order alloying elements in the SM²ART database and are not shown

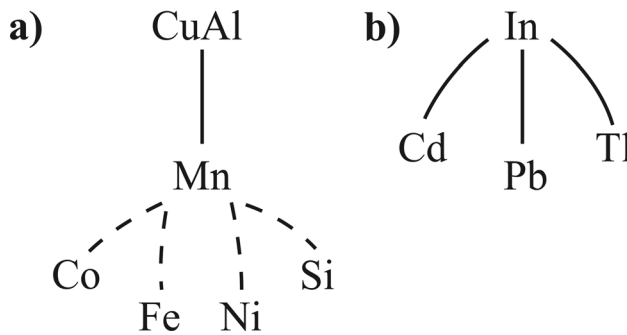


Fig. 12 **a** CuAl-based and **b** In-based alloys and elemental aggregates. Dashed lines indicate possible higher-order alloying elements

own, magnesium has an HCP structure with high plastic anisotropy, which results in poor plastic deformability at room temperature, limiting the viable uses of the material [123]. The addition of Sc to Mg results in a β -type structure, which improves the mechanical response of Mg alloys [120–128]. Magnesium alloys are used today in the automotive and consumer electronics industries as they are lightweight, resistant to corrosion, and have good castability [123, 126]. With these qualities, an Mg alloy that can also exhibit shape memory properties is of interest to the aerospace industry; however, due to the infancy of this alloy in the shape memory field, there are as of yet no known applications.

NiAl-Based and NiTa-Based Alloys

Nickel–aluminum-based SMAs are of high interest to the shape memory field due to their high melting point, high transformation temperatures, low density, excellent resistance to corrosion and oxidation, and ability to maintain strength at elevated temperatures. The ordered B2 structure of NiAl alloys also leads to materials that are very brittle at room temperature [129–136], making them difficult to use for applications. It is well known that after quenching rapidly from a high temperature, NiAl alloys containing 60 to 69 at.% Ni content can undergo transformation from a

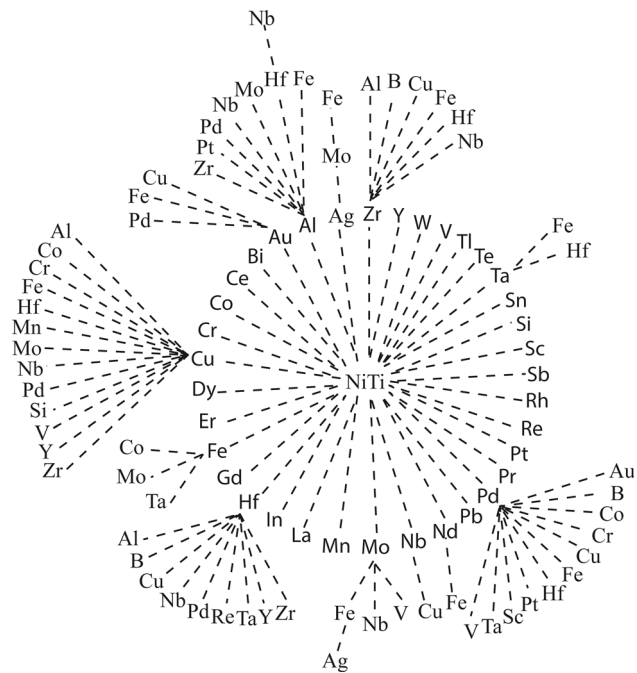


Fig. 14 NiTi-based alloys and elemental aggregates. Dashed lines indicate possible higher-order alloying elements

B2 (β -phase) structure to metastable L10 structure with either 3R or 7R stacking [130, 137]. Varying the Ni content from 60 to 69 at.% increases the transformation temperature of binary NiAl from -150 to $925\text{ }^{\circ}\text{C}$ [132, 138], with most interest in stable high transformation temperature alloys from systems containing 63 to 65 at.% Ni content, resulting in a martensitic transformation temperature of around $500\text{ }^{\circ}\text{C}$ [130, 137].

Various methods have been used in attempts to improve the ductility of NiAl at room temperature. The use of Pt-modified NiAl bond coating has been shown to improve oxidation resistance of B2 NiAl through the formation of an Al_2O_3 scale that strengthens the NiAl material [131, 132, 139]. The addition of other elements (Re, Fe, Co, Gd, Mn, Ti) has also been shown to reduce the

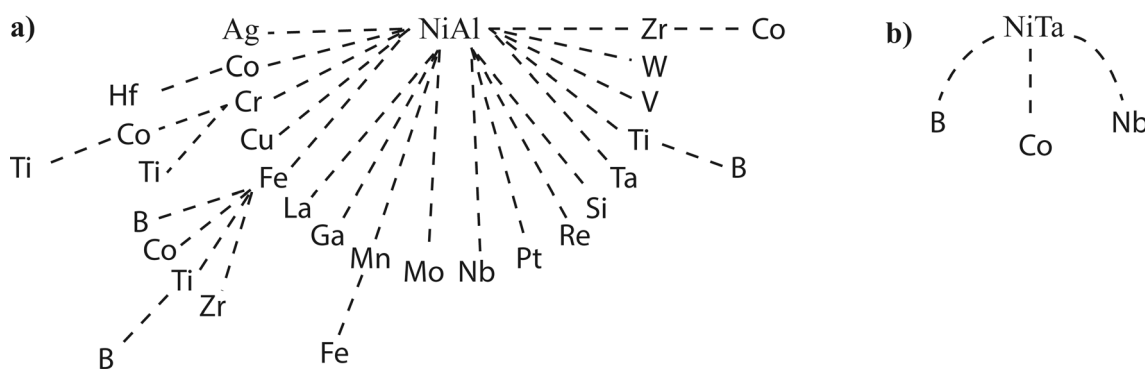


Fig. 13 **a** NiAl-based and **b** NiTa alloys and elemental aggregates. Dashed lines indicate possible higher-order alloying elements

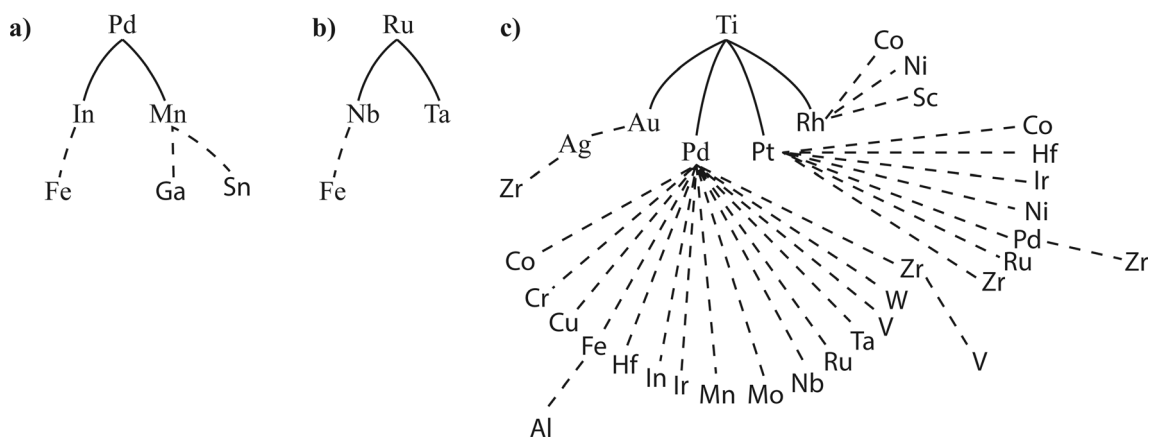


Fig. 15 a Pd-based, b Ru-based, and c Ti-based alloys and elemental aggregates. Dashed lines indicate possible higher-order alloying elements

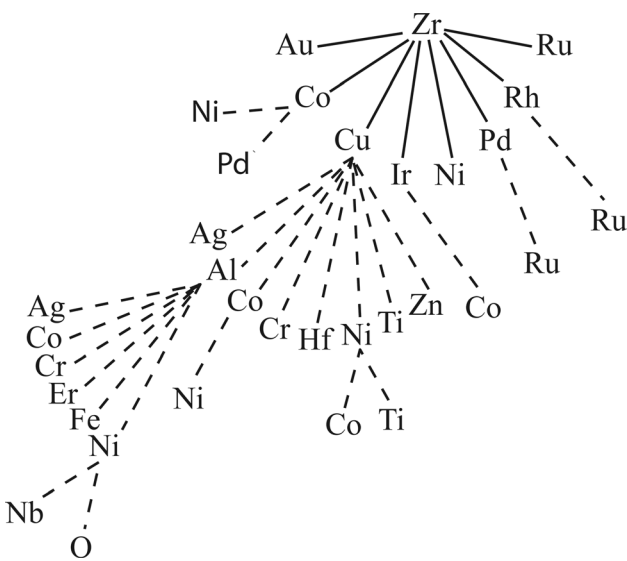


Fig. 16 Available alloys for the Zr-based system in the SM²ART database. Dashed lines indicate possible additional alloys

brittleness of binary NiAl through the formation of additional precipitates [129, 130, 137, 140–143]; however, this can also result in a decrease in the transformation temperatures. If a magnetic element is used (Fe, Co, Gd), it can result in a ferromagnetic shape memory alloy (FSMA) capable of magnetic-field-induced transformation [144] with strains as large as 6% or more, but FSMA are often brittle [145, 146].

NiAl coatings are commonly used in gas turbine engines due to their high melting point and strength at elevated temperatures, but they are not used in the form of SMAs.

NiTa alloys are of high interest due to their corrosion resistance, mechanical properties, high glass-forming ability, and high-temperature shape memory alloy (HTSMA) capabilities [147–153]. A HTSMA is loosely defined as an alloy with a martensitic transformation temperature greater than 100 °C. In NiTa alloys, as with most

HTSMAs, high transformation temperatures lead to brittle-like behavior at room temperature, which limits potential applications of the material. NiTa is widely studied today for use as superalloys, bulk metallic glasses, and SMAs. Ta is typically distributed into the γ' phase, which can increase resistance to oxidation and hot corrosion [153]. Ni_3Ta undergoes a monoclinic martensite to tetragonal austenite transformation [148, 149, 153].

NiTi-Based Alloys

NiTi-based alloys are among the most commonly used SMAs for a number of reasons. Binary NiTi is biocompatible, easy to process compared with other SMAs, and capable of large variations in transformation temperatures, which are achievable through adjustments to Ni content. Binary NiTi has high transformation stability and good strength and ductility. Due to its early discovery and biocompatibility, NiTi-based alloys have been the focus of significant research in the biomedical industry for use as stents, orthodontic wire, and more [1–16]. The high interest of NiTi alloys for biomedical use is one of the main driving factors that have helped advance the discovery and development of NiTi alloys beyond any other system to date. Binary NiTi is capable of two transformation paths from low-temperature martensite to high-temperature austenite. Solution-treated NiTi can undergo a B19' (monoclinic) to B2 (cubic) transformation upon heating [154, 155], whereas aging NiTi at the right temperature (400 °C, for example) or adding other elements (such as Fe) will cause the material to undergo a B19' (monoclinic) to R (trigonal) to B2 (cubic) transformation upon heating [156]. It is also known that the addition of other elements, such as Cu or Pd, will induce a B19 (orthorhombic) to B2 transformation path [156].

One of the primary benefits of binary NiTi is the wide range of transformation temperatures achievable by

increasing the Ni content. Increasing Ni content from roughly 49.7 to 51 at.% will decrease the M_s transformation temperature from 70 to -60 °C, as shown by Frenzel et al. [157]. Addition of other elements will also alter the transformation temperatures of the system so that it can be tailored to specific application requirements. For additional reading on the NiTi system, please refer to the work by Otsuka et al. [156].

The versatility of the NiTi system has resulted in many applications for a number of different alloys. Most prevalent are biomedical applications [1–16], followed by applications in various toys and automobiles [158–163]. Many additional applications exist for use in aircraft, spacecraft, and many others [17–20].

Pd-Based, Ru-Based, and Ti-Based Alloys

Pd-based alloys offer excellent mechanical properties, the potential for biocompatibility, and elastocaloric or ferromagnetic use applications [164–166]. Pd alloys are capable of A_f temperatures from -150 to 100 °C. The addition of other elements can help stabilize the transformations for a desired application. For more information, see references [164–171]. As the use of biomedical devices continues to increase and the footprint of such devices continues to decrease, it is essential to have SMAs that are high contrast for x-ray projection, and Pd-based alloys are good candidates for this, as demonstrated by their frequent use in dental devices.

Ru-based alloys exhibit very high transformation temperatures, up to 1200 °C in certain alloy configurations, leading some researchers to refer to them as “ultra-high-temperature shape memory alloys” (UHTSMAs). RuTa and RuNb alloys have M_s temperatures ranging from 400 to 1200 °C, depending on the composition [172–174]. Equiautomic RuNb and RuTa alloys are known to exhibit a two-stage phase transformation from low-temperature monoclinic β'' to tetragonal β' and finally to a β (B2, cubic) structure [174–177]. Like other HTSMAs, Ru alloys typically do not demonstrate good mechanical properties at elevated temperature, which makes them unviable for many applications; however, the addition of other elements may help improve the stability of these alloys at room temperatures [178, 179]. Due to the very high transformation temperatures, these alloys may be viable for many high-temperature applications, such as use in gas turbine engines, combustion engines, rocket engines, hypersonic devices, or nuclear reactors.

In the SM²ART database there are currently four main secondary alloys for the Ti-based alloys: Au, Pd, Pt, and Rh. Due to their unique properties of biocompatibility and high-temperature transformation capabilities, these alloys are of high interest for a wide range of applications ranging

from biomedical to turbine engines. TiAu-based alloys are of specific interest, as they are both biocompatible and capable of high-temperature transformation, allowing for a large range of applications [180, 181].

TiPd alloys have been researched extensively as they are known to have good stability in the binary state; the addition of ternary elements furthers stability and can be used to tailor transformation temperatures [182–185]. TiPd SMAs are known to undergo a B2 to B19 transformation around 525 °C from cooling [182, 186, 187]. The addition of other elements (such as iron) enables increased fatigue life and durability while decreasing transformation temperatures [188].

The combination of Ti and Pt results in a transformation temperature of roughly 1050 °C, one of the highest known temperature transformations in SMAs (apart from Ru alloys) [189–192], but the high cost associated with this element pairing can be an impediment to its use. The addition of other elements is known to help stabilize TiPt and increase fatigue life [192–194].

The addition of Rh to Ti induces a second phase transformation; the first is from B2 to L_{10} at around 740 °C, and the second is from L_{10} to $B1'$ at around 345 °C [195].

UNb Alloys

UNb alloys are of interest in the nuclear energy field due to their high corrosion resistance, good ductility, and good mechanical properties [196–199]. UNb alloys with a niobium content between 10 and 16 at.% are known to have an α'' (monoclinic) structure and exhibit the SME; alloys with niobium content between 16 and 20 at.% have a γ^0 (tetragonal) structure and are also known to exhibit the SME [196, 198–203].

Zr-Based Alloys

Zirconium-based alloys can function as HTSMAs with potential for use in manufacturing, energy, automotive, and aerospace industries. There has been considerable interest in these alloys due to good high-temperature casting fluidity and workability, and they are relatively low in cost compared with many other HTSMAs [204, 205]. Zr-based alloys have martensite transformation temperatures ranging from around 100 °C up to 1450 °C [204–210]. ZrCu-based intermetallic compounds and binary ZrCu are both known to undergo martensitic transformation from high-temperature B2 into two monoclinic martensitic structures (superstructures with Cm symmetry or B19' with P2₁/m symmetry) [204, 205, 207]. Equiautomic ZrPd also undergoes two phase changes: B2 to orthorhombic CrB at an M_s of 540 °C, leading to monoclinic martensite at room temperature [211].

Superelastic Alloys

Superelastic (SE) alloys have been widely used in the biomedical industry for stents [1, 2], dentistry tools, orthodontic wires [3–16] and other devices due to their ability to recover large strains and maintain a relatively constant stress. These medical alloys with similar or modified compositions have also found use in other applications such as industrial applications (e.g., bridges, building), terramechanics (e.g., non-pneumatic tires), marine research [212], and tribological components (e.g., bearings, bushings, cutlery, and blades) [213, 214]. Within the SM²ART database, the primary focus was toward NiTi-based alloys for tribological applications with seven ternary or higher elemental addition comprising of NiTiAl, NiTiCr, NiTiHf, NiTiNb, NiTiTa, and NiTiZr. A key property pertinent to these alloy systems is hardness as shown in Fig. 17. Based on the Ni content, production method, or the heat treatments used, all of which are also available within the SM²ART database, an alloy chemistry and associated processes can be gleaned from this information to yield a desired property.

Magnetic Shape Memory Alloys

MSMAs are a class of SMAs that are capable of mechanical transformation within a magnetic field in addition to thermally induced transformation. MSMAs demonstrate recoverable deformations around 6 to 10% strain, similar to SMAs; however, the response time for transformation when introduced to a magnetic field is on the order of milliseconds, significantly faster than

response time for thermally activated SMAs. This transformation frequently requires very large magnetic fields for actuation to occur in these materials, and single crystals are unavoidable, making the use of MSMAs limited for applications and expensive to manufacture.

The two main MSMA base systems studied today are NiMn and FePd, with the most widely studied alloy being NiMnGa. Currently, only the NiMn system is available in the SM²ART database. The ternary additions available for NiMn alloys in the SM²ART database are shown in Fig. 18. Due to the number of data points, the information was split into two plots so all data could be visualized. The ternary element is correlated to the name and symbols listed in the legend above the plots.

Nonmetallic Shape Memory Materials

Although the variety and versatility of SMAs make them advantageous for use in numerous applications, SMAs are not always feasible for a given design. Significant research has thus been conducted into other forms of SMMs, such as SMPs and SMCs. These other materials have unique abilities outside of the capabilities of SMAs. SMPs can be bonded with other polymers much more easily than metals and can thus be more readily used in infusion applications to create composite materials. SMCs are capable of very high transformation temperatures (up to 1225 °C) while also maintaining significant strength, with critical stresses over 4 GPa. A brief overview of these materials systems and their capabilities is provided in the following sections.

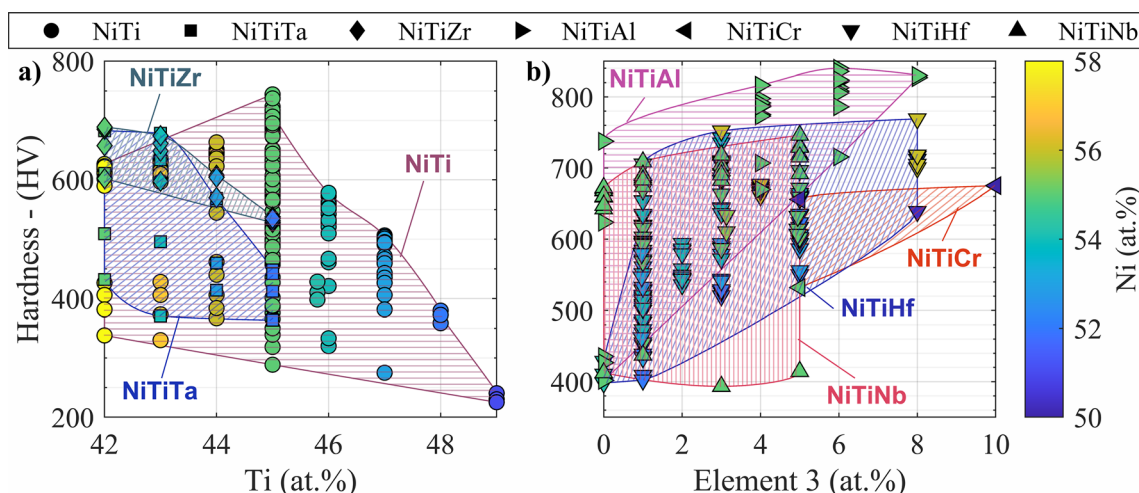


Fig. 17 Hardness of various SE alloys. **a** Shows the hardness for NiTi, NiTiTa, and NiTiZr and **b** shows the hardness for NiTiAl, NiTiCr, NiTiHf, and NiTiNb

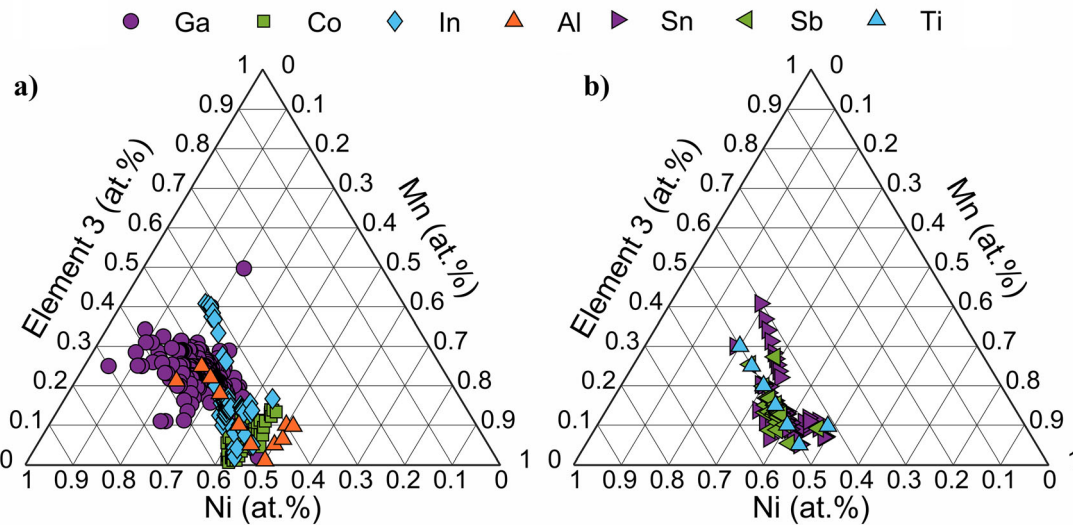


Fig. 18 NiMn MSMA ternary diagrams showing available compositions in the SM²ART database

Shape Memory Polymers

The first SMP was patented in 1971 by Radiation Applications Inc [215]. This SMP and others developed around this time were significantly limited due to difficulties processing the material. Once thermoplastic polyurethane (TPU) SMPs were developed, their wide glass transition temperatures (T_g) and easy processability greatly increased interest in SMPs. SMPs and SMAs share many potential applications, such as applications for use in the biomedical, aerospace, and automotive industries. SMAs (specifically NiTi-based SMAs) have dominated the shape memory industry for a number of reasons, most importantly for their good mechanical properties, great shape memory ability, easy processability, and biocompatibility. Compared with SMPs, however, traditional SMAs are generally heavier, stiffer, and more costly; they also have a low rate of deformation and are not biodegradable, making them unfit for many applications. SMPs are typically easier to process; are lower in cost, toxicity, and density; have much more significant recoverable strains (as much as 800%), and, when coupled with other SMPs, are capable of multiple transformations. SMPs are also capable of transformation from a number of external stimuli, such as heat, UV light, magnetic fields, electrical fields, and pH [216–221].

Thermally induced SMPs undergo shape change through a combination of cross-links and switching segments. Cross-links are the SMP components that define the permanent shape and inhibit slipping of the polymer chains. Switching segments absorb externally applied stresses and maintain any temporary deformations [222, 223]. Once deformed, the SMP is capable of recovered deformation through chemical or physical stimuli that form temporary

reversible cross-links. In the case of thermally induced SMPs, the solidification of switching segments creates physical cross-links in which energy can be stored. After deformation, upon heating the SMP past the melting or glass transition point, the cross-links will melt or soften, releasing the stored energy in the polymer chains and driving the SME.

The distinct mechanisms and properties of SMPs illustrate the importance for a single source for data. With numerous chemical combinations possible, comparing and designing with SMPs can be a burdensome task, which is remediated with the SM²ART database which currently contains over 89 SMP chemical families. Figure 19 shows the fixity percentage for all SMPs in the SM²ART database with available data. The fixity is indicative of a material's ability to recover from mechanical deformation and is an important metric for SMPs. As seen in this figure, many polymers exist that have very little variation from 100%, showing the capabilities of shape fixing with SMPs.

Figure 20 shows the recovery versus recovery temperature for all SMPs in the SM²ART database with data available for this metric. The recovery of SMPs is indicative of the materials' ability to memorize the permanent shape set. In the figure, many systems show recoveries above 100%, which indicates the material recovered past the initial set shape. SMPs are capable of a wide range of recovery temperatures, as low as -100 °C, as indicated in Fig. 20e in the styrenic block copolymer system, and up to 400 °C, as observed in Fig. 20a in the polyimide system. The wide range of temperatures available for SMPs, along with their higher strain capabilities as compared with SMAs, further demonstrates the unique abilities and possible applications of these materials.

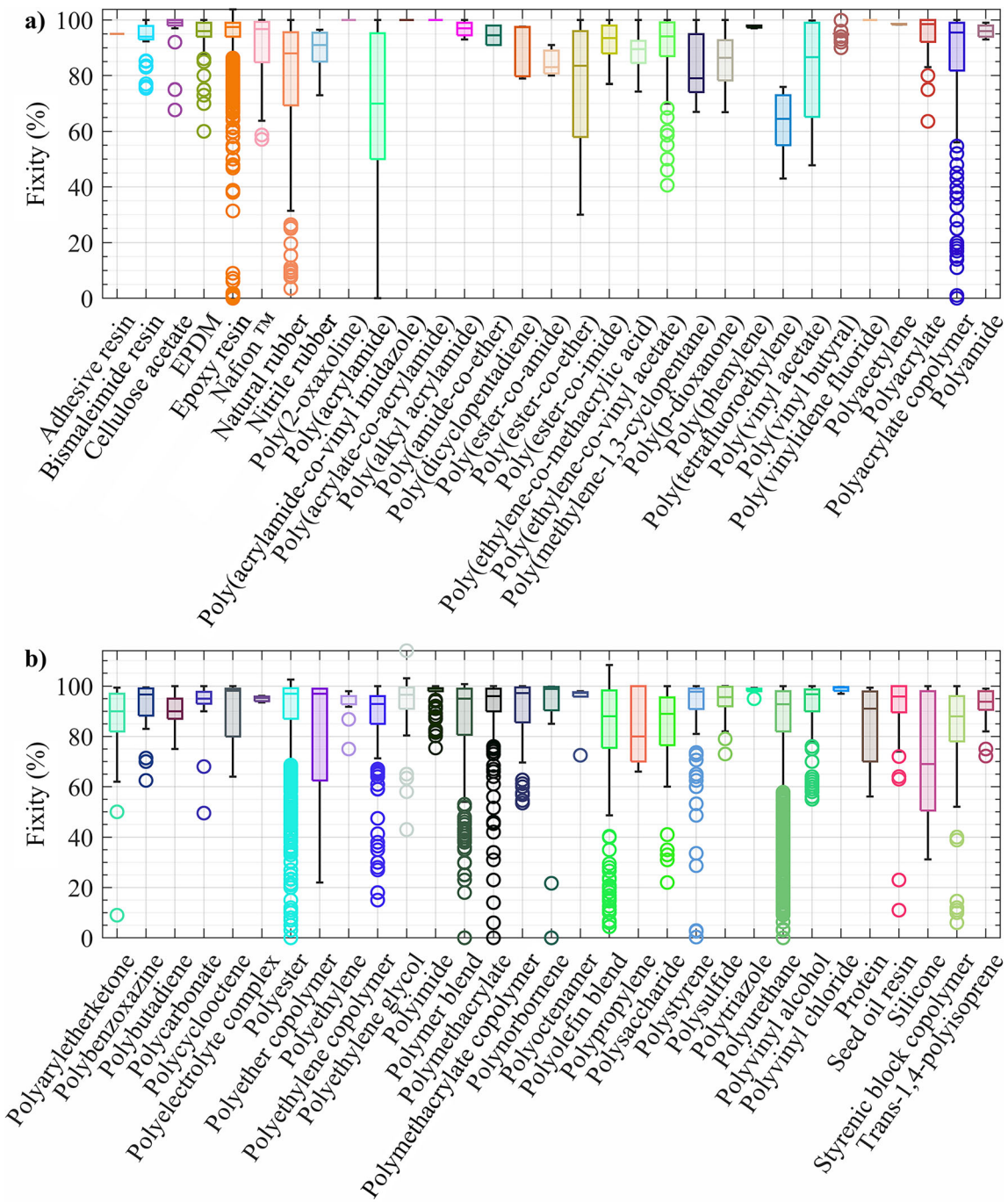


Fig. 19 Fixity (%) parameter of all available SMP systems in the SM²ART database

SMPs have numerous applications in the biomedical, textile, and aerospace industries. Clot removal devices, vascular stents, orthodontic appliances, sutures, and dialysis needles have been suggested as possible biomedical applications [28–35]. Research into SMPs for use in textile applications has included experiments with fabrics that unwrinkle with low heat, fabrics that adjust fit and

breathability based on body heat from the wearer, and fabrics capable of absorbing impact forces to protect passengers from impact during a crash [36–40]. The aerospace industry has numerous applications, with deployable solar arrays and truss systems, deployable antennas, and morphing structures as researched possibilities [41–48].

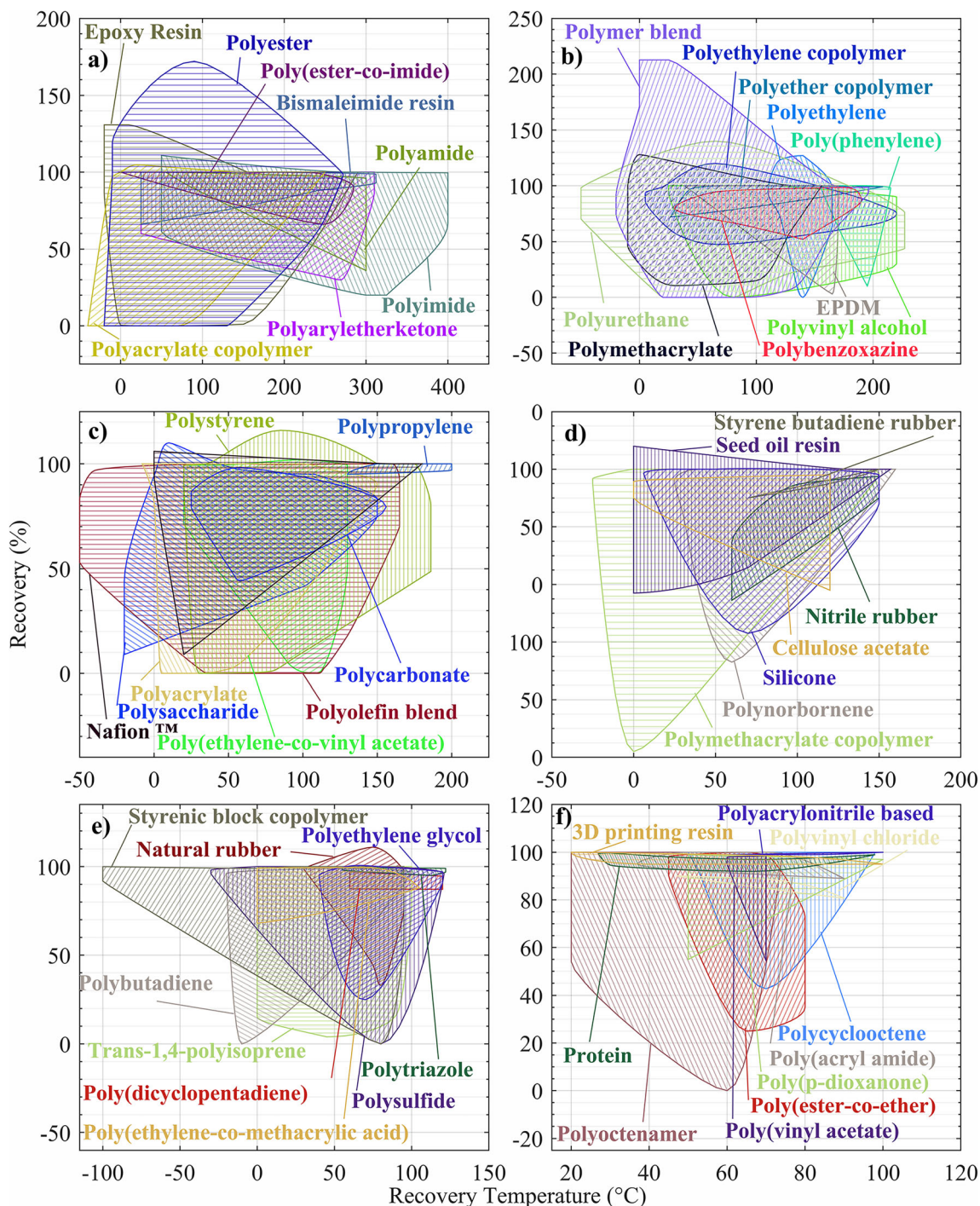


Fig. 20 Recovery (%) versus recovery temperature for all SMP systems with available data in the SM²ART database

Shape Memory Ceramics

The SME was first observed in ceramics in 1988 by Reyes-Morel et al. [224]. Based on the composition of the SMC, the SME can be induced thermally, ferroelectrically, ferromagnetically, or by applying stress. A number of ceramic- and intermetallic-based systems are capable of

thermally induced transformation, including zirconia, alumina, mica, silicon carbide, and silicon nitride. Mica-based glass-ceramics are capable of the largest strain recovery among these materials, up to 0.5% at elevated temperatures [225]. Zirconia ceramics are known for good stress-induced shape recovery; this occurs when the material is stressed above the A_f temperature, which induces a

martensitic response until the stress is released. The phase transformation of zirconia ceramics occurs between a tetragonal and monoclinic structure [225]. Fe-based ceramics are known for ferromagnetic SME capabilities.

SMCs provide a number of benefits over SMAs. Although SMAs do have higher strain tolerance (SMCs begin to crack at around 2% strain, whereas typical SMAs can withstand strains ranging from 2 to 5%) SMCs are very stable at high temperatures of up to 1200 °C. At these higher temperatures, they maintain strength and hardness and are corrosion resistant, which is not the case for many SMAs. Due to the tetragonal-monoclinic transformation zirconia undergoes, it is possible to obtain up to 15% shear strains with these ceramics [225]. Figure 21 shows a snapshot of the transformation temperature capabilities of the zirconia system with various doped elemental additions. The ZrO₂Ce system provides a wide range of transformation temperatures, with a near-zero austenitic transformation on the low end to over 1200 °C on the high end. Combining zirconia with other doped elements provides a similar variation, but the austenitic transformation temperatures start around 600 to 800 °C. These high-temperature transformations are only present in a select number of SMAs and, due to oxidation, can cause the alloys to be brittle. This is not the case with SMCs, which maintain their strength at elevated temperatures.

One of main the benefits of SMCs is that alongside the high-temperature transformations come very high-strength capabilities. Figure 22 illustrates this, indicating a maximum stress of over 3 GPa in bulk material for ZrO₂Ce (Fig. 22a) and almost 5 GPa for micropillar tests on ZrO₂Y

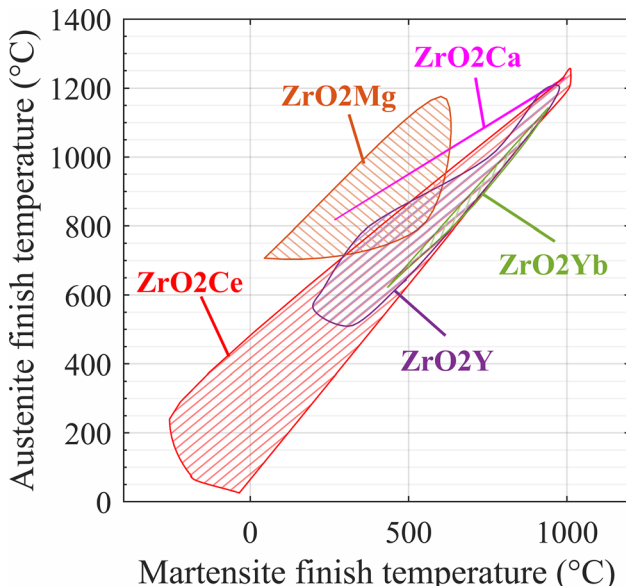


Fig. 21 A_f and M_f transformation temperatures for ZrO₂-based shape memory ceramics

samples (Fig. 22b). Compared to SMAs, which typically have maximum stresses around 1 GPa, SMCs are capable of both high-temperature transformation and very high strength (though are brittle) and as such are promising for numerous high-strength applications.

Current applications for SMCs include latching relays and mechanical clamps. Uchino et al. developed a latching relay using an antiferroelectric ceramic known as PZNST [49]. This relay requires an electrical pulse less than 5 ms in order to operate, which is faster than traditional piezoelectric applications. Other applications in aeronautics, automotive, and biomedical industries may be possible with SMCs, although brittleness must be taken into consideration when designing with these materials.

Conclusions and Next Steps

The Shape Memory Materials Analysis and Research Tool (SM²ART) database is a unique, powerful tool with data from over 2500 peer-reviewed articles and published company results [56] collected in a single location. Users can easily access data on shape memory alloys (SMAs), superelastic (SE) alloys, magnetic shape memory alloys (MSMAs), shape memory polymers (SMPs), and shape memory ceramics (SMCs). The SM²ART database provides users with the ability to plot data from any of these material systems and compare valuable metrics, such as transformation temperatures, heat treatments, and hysteresis. The SM²ART database is also capable of scatter, box-and-whisker, ternary, and sunburst plots, providing researchers and material developers powerful information for designing and using SMMs. Along with these plotting tools, the SM²ART database offers a variety of analysis tools, such as regression fitting, k-means clustering, and data filters.

The SM²ART database gives users ready access to invaluable information that was previously only accessible through tedious searches of countless publications. Using the SM²ART database, researchers and material engineers can easily compare multiple alloy and material systems, identify gaps in the current SMM research, and quickly determine potential alloys for a specific application. Materials scientists can also use the data and trends identified in the database to design new alloys using an informed approach, saving significant time, money, and resources.

The SM²ART database is not limited to metal alloys but also provides information on polymer and ceramic systems known to exhibit the SME. These alternative SMM systems provide their own unique benefits: SMPs are capable of multi-shape memory systems coupled in one combined

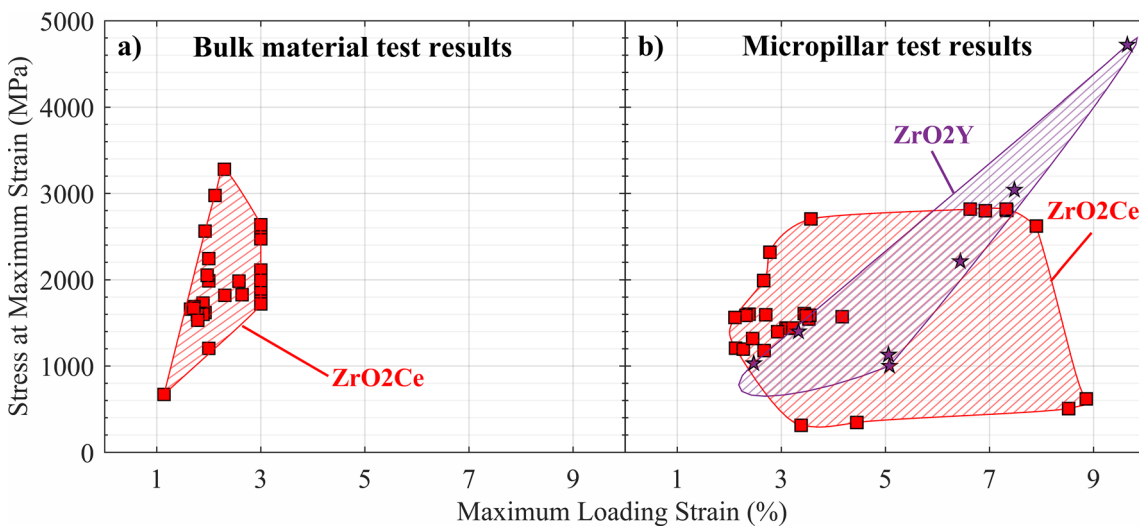


Fig. 22 Stress versus strain for shape memory ceramics. **a** Bulk material test results. **b** Micropillar test results

polymer system, and SMCs have high-temperature, high-strength capabilities beyond those of traditional SMAs.

A number of useful features are being developed to further enhance the capabilities of the SM²ART database. Future releases will make it possible for users to permanently add their published data to the database. Machine learning will also be incorporated to aid in the development of new materials. Special topics such as additive manufacturing a single crystal modules are also under development and will be deployed upon completion. Current version of this SM²ART database can be access via this web url: https://shapememory.grc.nasa.gov/shape_memory_alloys.

Acknowledgements Funding from the NASA Aeronautics Research Mission Directorate (ARMD) Transformational Tools and Technologies (TTT) project is gratefully acknowledged. The authors wish to thank Tyler Kujawa, Daniel D. Kilkenny, Sean A. Bostik, Ron Gould, and Edward A. Jones for their contributions in the software development that made the SM²ART database possible. The authors also thank Joshua Stuckner and Ian S. Howell for their contributions toward the analytical tools in the database, and Glen Bigelow and Darrell Gaydosh for content and reviews of the database. The authors also thank student interns Avery Young and Faith Gantz at the University of North Texas, William Treherne at Texas A&M University, Lina V. Daza at the University of Puerto Rico—Mayaguez, and Julie Foroosh at the University of Central Florida for data collection and extraction for the shape memory alloy section in the database. The authors also thank Hang Yu and Hunter Rauch from the Virginia Technical Institute for their contributions toward the shape memory ceramics section in the database, Kevin A. Cavicchi and Sayan Basak at the University of Akron for their contributions toward the shape memory polymers section in the database, Mohammad Elahinia and Parisa Bayati at the University of Toledo for their contributions toward the superelastic alloys section in the database, Ibrahim Karaman and William Treherne at Texas A&M University for their contributions toward CuAl alloys in the database, and Haluk E. Karaca, Guher P. Toker, and Sayed Ehsan Saghaian at the University

of Kentucky for their contributions toward the magnetic shape memory alloy section in the database.

References

- Takagi T, Sutou Y, Kainuma R, Yamauchi K, Ishida K (2006) Effect of prestrain on martensitic transformation in a Ti_{46.4}Ni_{47.6}Nb_{6.0} superelastic alloy and its application to medical stents. *J Biomed Mater Res B* 76(1):179–183
- Tian Y, Yu Z, Ong CYA, Kent D, Wang G (2015) Microstructure, elastic deformation behavior and mechanical properties of biomedical β-type titanium alloy thin-tube used for stents. *J Mecha Behav Biomed Mater* 45:132–141
- McCoy B (1996) Comparison of compositions and differential scanning calorimetric analyses of the new copper-Ni-Ti wires with existing Ni-Ti orthodontic wires [Thesis], The Ohio State University, p 111
- Gil F, Planell J (1999) Effect of copper addition on the superelastic behavior of Ni-Ti shape memory alloys for orthodontic applications. *J Biomed Mater Res* 48(5):682–688
- Mitose K, Ueki T (1999) Ni-Ti-Pd superelastic alloy material, its manufacturing method, and orthodontic archwire made of this alloy material, U.S. Patent No. 5,885,381.
- Iijima M, Ohno H, Kawashima I, Endo K, Mizoguchi I (2002) Mechanical behavior at different temperatures and stresses for superelastic nickel-titanium orthodontic wires having different transformation temperatures. *Dent Mater* 18(1):88–93
- Suzuki A, Kanetaka H, Shimizu Y, Tomizuka R, Hosoda H, Miyazaki S, Okuno O, Igarashi K, Mitani H (2006) Orthodontic buccal tooth movement by nickel-free titanium-based shape memory and superelastic alloy wire. *Angle Orthod* 76(6):1041–1046
- Biermann MC, Berzins DW, Bradley TG (2007) Thermal analysis of as-received and clinically retrieved copper-nickel-titanium orthodontic archwires. *Angle Orthod* 77(3):499–503
- Kanetaka H, Shimizu Y, Hosoda H, Tomizuka R, Suzuki A, Urayama S, Inamura T, Miyazaki S, Takano-Yamamoto T (2007) Orthodontic tooth movement in rats using Ni-free Ti-based shape memory alloy wire. *Mater Trans* 48(3):367–372
- Pun DK, Berzins DW (2008) Corrosion behavior of shape memory, superelastic, and nonsuperelastic nickel-titanium-

- based orthodontic wires at various temperatures. *Dent Mater* 24(2):221–227
11. Wang QY, Zheng YF (2008) The electrochemical behavior and surface analysis of $Ti_{50}Ni_{47.2}Co_{2.8}$ alloy for orthodontic use. *Dent Mater* 24(9):1207–1211
 12. Zheng YF, Wang QY, Li L (2008) The electrochemical behavior and surface analysis of $Ti_{49.6}Ni_{45.1}Cu_5Cr_{0.3}$ alloy for orthodontic usage. *J Biomed Mater Res B* 86(2):335–340
 13. Phukaoluan A, Khantachawana A, Kaewtatip P, Dechkunakorn S, Anuwongnukroh N, Santiwong P, Kajornchaiyakul J (2011) Property improvement of TiNi by Cu addition for orthodontics applications. *Appl Mech Mater* 87:95–100
 14. Arciniegas M, Manero J, Espinar E, Llamas J, Barrera J, Gil F (2013) New Ni-free superelastic alloy for orthodontic applications. *Mater Sci Eng C* 33(6):3325–3328
 15. Phukaoluan A, Dechkunakorn S, Anuwongnukroh N, Khantachawana A, Kaewtatip P, Kajornchaiyakul J, Wichai W (2017) Loading and unloading forces following addition of 5% Cu in nickel-titanium alloy used for orthodontics, key engineering materials. *Trans Tech Publ*, pp 161–166
 16. Barros CDDR, Gomes JADCP (2021) Influence of Cu addition and autoclave sterilization on corrosion resistance and biocompatibility of NiTi for orthodontics applications. *Mater Res*. <https://doi.org/10.1590/1980-5373-mr-2020-0369>
 17. Hartl DJ, Lagoudas DC (2007) Aerospace applications of shape memory alloys. *Proc Inst Mech Eng G* 221(4):535–552
 18. Bovesecci G, Corasaniti S, Costanza G, Tata ME (2019) A novel self-deployable solar sail system activated by shape memory alloys. *Aerospace* 6(7):78
 19. Costanza G, Tata ME (2020) Shape memory alloys for aerospace, recent developments, and new applications: a short review. *Materials* 13(8):1856
 20. Vertegaal CJC, Bentum MJ, Pourshaghghi HR (2021) Using shape memory alloy for cubesat antenna design in space. In: 2021 15th European conference on antennas and propagation (EuCAP), pp 1–5
 21. Monroe J, McAllister J, Content D, Zgarba J (2020) Negative thermal expansion ALLVAR alloys for smaller optics. *SPIE Photonics West*, San Francisco, California, February 4–6 2020
 22. Monroe J, East M, Hull T (2021) ALLVAR alloy athermalization: a novel and cost-effective alternative for small to moderate sized space telescopes. *SPIE Photonics West*, Bellingham, Washington, March 6–11 2021
 23. Clarke AJ, Field RD, McCabe RJ, Cady CM, Hackenberg RE, Thoma DJ (2008) EBSD and FIB/TEM examination of shape memory effect deformation structures in U–14at.% Nb. *Acta Mater* 56(11):2638–2648
 24. Clarke AJ, Field RD, Dickerson PO, McCabe RJ, Swadener JG, Hackenberg RE, Thoma DJ (2009) A microcompression study of shape-memory deformation in U–13at.% Nb. *Scr Mater* 60(10):890–892
 25. Rashidi S, Ehsani MH, Shakouri M, Karimi N (2021) Potentials of magnetic shape memory alloys for energy harvesting. *J Magn Magn Mater* 537:168112
 26. Kohl M, Joseph J, Seigner L (2022) Energy harvesting using magnetic shape memory alloys. In: Olabi A-G (ed) Encyclopedia of smart materials. Elsevier, Oxford, pp 96–103
 27. Zhang X, Qian M (2022) Application of magnetic shape memory alloys. In: Zhang X, Qian M (eds) Magnetic shape memory alloys: preparation, martensitic transformation and properties. Springer, Singapore, pp 255–268
 28. Small W, Metzger MF, Wilson TS, Maitland DJ (2005) Laser-activated shape memory polymer microactuator for thrombus removal following ischemic stroke: preliminary in vitro analysis. *IEEE J Sel Top Quantum Electron* 11(4):892–901
 29. Maitland DJ, Metzger MF, Schumann D, Lee A, Wilson TS (2002) Photothermal properties of shape memory polymer micro-actuators for treating stroke*. *Lasers Surg Med* 30(1):1–11
 30. Chen M-C, Chang Y, Liu C-T, Lai W-Y, Peng S-F, Hung Y-W, Tsai H-W, Sung H-W (2009) The characteristics and in vivo suppression of neointimal formation with sirolimus-eluting polymeric stents. *Biomaterials* 30(1):79–88
 31. Baer GM, Small W, Wilson TS, Benett WJ, Matthews DL, Hartman J, Maitland DJ (2007) Fabrication and in vitro deployment of a laser-activated shape memory polymer vascular stent. *Biomed Eng Online* 6(1):43
 32. Jung YC, Cho JW (2010) Application of shape memory polyurethane in orthodontic. *J Mater Sci—Mater Med* 21(10):2881–2886
 33. Nakasima A, Hu JR, Ichinose M, Shimada H (1991) Potential application of shape memory plastic as elastic material in clinical orthodontics. *Eur J Orthod* 13(3):179–186
 34. Lendlein A, Langer R (2002) Biodegradable, elastic shape-memory polymers for potential biomedical applications. *Science* 296(5573):1673–1676
 35. Ortega JM, Small W, Wilson TS, Benett WJ, Loge JM, Maitland DJ (2007) A shape memory polymer dialysis needle adapter for the reduction of hemodynamic stress within arteriovenous grafts. *IEEE Trans Biomed Eng* 54(9):1722–1724
 36. Gök MO, Bilir MZ, Gürcüm BH (2015) Shape-memory applications in textile design. *Procedia Soc Behav Sci* 195:2160–2169
 37. Hu J, Chen S (2010) A review of actively moving polymers in textile applications. *J Mater Chem* 20(17):3346–3355
 38. Hu J, Meng H, Li G, Ibekwe SI (2012) A review of stimuli-responsive polymers for smart textile applications. *Smart Mater Struct* 21(5):053001
 39. Jeong HM, Ahn BK, Cho SM, Kim BK (2000) Water vapor permeability of shape memory polyurethane with amorphous reversible phase. *J Polym Sci B* 38(23):3009–3017
 40. Ding XM, Hu JL, Tao XM, Wang ZF, Wang B (2005) Free volume and water vapor transport properties of temperature-sensitive polyurethanes. *J Polym Sci B* 43(14):1865–1872
 41. Yin WL, Sun QJ, Zhang B, Liu JC, Leng JS (2008) Seamless morphing wing with SMP skin. *Adv Mater Res* 47–50:97–100
 42. Barrett R, Taylor R, Keller P, Codell D, Adams L (2007) Deployable reflectors for small satellites. *Small Satellite Conference*, Logan, Utah, August 4–9
 43. Barrett R, Taylor R, Keller P, Lake M, Stern T, Freebury G, Beidleman N (2007) Design of a solar array to meet the standard bus specification for operation responsive space. In: 48th AIAA/ASME/AHS/ASC structures, structural dynamics, and materials conference, p 2332
 44. Yin W, Liu J, Leng J (2009) Deformation analysis of shape memory polymer for morphing wing skin under airflow. *Front Mech Eng China* 4(4):447
 45. Zhang R, Guo X, Liu Y, Leng J (2014) Theoretical analysis and experiments of a space deployable truss structure. *Compos Struct* 112:226–230
 46. Lan X, Liu Y, Lv H, Wang X, Leng J, Du S (2009) Fiber reinforced shape-memory polymer composite and its application in a deployable hinge. *Smart Mater Struct* 18(2):024002
 47. Hager MD, Bode S, Weber C, Schubert US (2015) Shape memory polymers: past, present and future developments. *Prog Polym Sci* 49–50:3–33
 48. Liu Y, Du H, Liu L, Leng J (2014) Shape memory polymers and their composites in aerospace applications: a review. *Smart Mater Struct* 23(2):023001
 49. Uchino K (2016) Antiferroelectric shape memory ceramics. *Actuators* 5(2):11

50. Quade DJ (2017) Investigation of interfacial bonding between shape memory alloys and polymer matrix composites. University of Akron, Orrville
51. Caltagirone PE (2021) Improvements of fiber reinforced thermoplastic composite bonds: thick joint failure model, shape memory alloy reinforcements, and in-situ x-ray characterizations, PhD thesis, Colorado School of Mines, Golden, Colorado
52. Soto-Parra D, Zhang X, Cao S, Vives E, Salje EKH, Planes A (2015) Avalanches in compressed Ti-Ni shape-memory porous alloys: an acoustic emission study. *Phys Rev E* 91(6):060401
53. Tang W, Cederström J, Sandström R (1991) Property database for the development of shape memory alloy applications. *J Phys IV Proc.* <https://doi.org/10.1051/jp4:1991419>
54. Smith R, Oates B (2022) Smart materials database. https://rsmith.math.ncsu.edu/Smart_Materials_Database/. Accessed 22 Nov 2022
55. Shape memory alloys. In: Davis JR (ed) (1998) Metals handbook desk edition, ASM International
56. Benafan O (2022) Shape memory materials database. <https://shapememory.grc.nasa.gov/>. Accessed 22 Nov 2022
57. Benafan O, Bigelow GS, Young AW (2020) Shape memory materials database tool—a compendium of functional data for shape memory materials. *Adv Eng Mater* 22(7):1901370
58. Honrao SJ, Benafan O, Lawson JW (2022) Data-driven study of shape memory behavior of multi-component Ni-Ti alloys in large compositional and processing space. *Shape Mem Superalst* 9:144–155
59. Krishnan R, Brown L (1973) Martensitic transformations in β Ag-Cd alloys. *Metall Trans* 4(4):1017–1022
60. Miura S, Horn F, Nakanishi N (1979) Pseudoelastic behaviour associated with thermoelastic martensitic transformation in an $\text{Au}_{52.5x}\text{Ag}_x\text{Cd}_{47.5}$ pseudobinary alloy. *Philos Mag A* 40(5):611–624
61. Nagasawa A, Tatsumi A (1988) Phase transformation in the quenched Ag_3Al beta phase alloy. *Trans Jpn Inst Met* 29(8):625–633
62. Prasad K, Bansal C (1986) Resistivity and thermoelectric power measurements on AgCd shape memory alloys. *Phys Status Solidi A* 98(2):453–464
63. Scherrer P, Rubini S, Dimitropoulos C, Borsa F (1995) Thermal cycling and growth of the martensite studied by NMR in an Ag-Cd alloy. *Le Journal de Physique IV*. <https://doi.org/10.1051/jp4:1995268>
64. Takezawa K, Hoshi H, Marukawa K (1999) Relation between long-range ordering and martensitic transformation temperature in Ag alloys. *Mater Sci Eng A* 273:564–567
65. Takezawa K, Sato S, Minato K, Maruyama S, Marukawa K (1992) Martensitic and bainitic transformations in Ag-Zn alloys. *Mater Trans JIM* 33(3):294–301
66. Tong H, Wayman C (1973) Marmem effect in $\beta'\text{AgCd}$ alloys. *Scr Metall* 7(2):215–221
67. Olander A (1932) An electrochemical investigation of solid cadmium-gold alloys. *J Am Chem Soc* 54:3819–3833
68. Battezzati L, Barbero S, Belotti M, Rontino G (2003) Resistometric and calorimetric analysis of phase transformations in AuCu alloys. *Z Met* 94(4):449–452
69. Cashion JD, Chadwick J, Coyle CM, Finlayson TR (2003) The aging effect in Au-Cd alloys: a Mössbauer spectroscopy study. *Journal de Physique IV (Proceedings)* EDP sciences 112:1087–1090
70. Emura Y, Ohba T, Otsuka K (1992) Crystal structure of ζ_2' Martensite in Au-49.5 at% Cd alloy. *MRS Online Proc Libr Arch.* <https://doi.org/10.1557/PROC-246-73>
71. Ishibashi H, Kogachi M, Ohba T, Ren X, Otsuka K (2002) Vacancy migration and long-range ordering due to ageing in AuCd shape memory alloys. *Mater Sci Eng A* 329:568–572
72. Kogachi M, Ishibashi H, Ohba T, Ren X, Otsuka K (2000) Examination of vacancy migration and long-range ordering due to ageing in Au-49.8Cd shape memory alloy. *Scr Mater* 42(9):841–847
73. Otsuka K, Ren X, Murakami Y, Kawano T, Ishii T, Ohba T (1999) Composition dependence of the rubber-like behavior in ζ_2' -martensite of AuCd alloys. *Mater Sci Eng A* 273:558–563
74. Xue D, Zhou Y, Ding X, Otsuka K, Sun J, Ren X (2011) Martensite aging effects on the dynamic properties of Au-Cd shape memory alloys: characteristics and modeling. *Acta Mater* 59(12):4999–5011
75. Miura S, Maeda S, Nakanishi N (1974) Pseudoelasticity in Au-Cu-Zn thermoelastic martensite. *Philos Mag* 30(3):565–581
76. Sakamoto H, Otsuka K, Shimizu K (1977) Rubber-like behavior in a Cu-Al-Ni alloy. *Scr Metall* 11(7):607–611
77. Abu-Arab A, Ahlers M (1988) The stabilization of martensite in Cu-Zn-Al alloys. *Acta Metall* 36(9):2627–2638
78. Battezzati L, Belotti M, Brunella V (2001) Calorimetry of ordering and disordering in AuCu alloys. *Scr Mater* 44(12):2759–2764
79. Hennig J, Mari D, Schaller R (2009) Order-disorder phase transition and stress-induced diffusion in Au-Cu. *Phys Rev B* 79(14):144116
80. Mašek P, Chmelik F, Šíma V, Brinck A, Neuhäuser H (1999) Microstructure processes induced by phase transitions in a CuAu alloy as studied by acoustic emission and optical cinematography. *Acta Mater* 47(2):427–434
81. Miranda G, Silva F, Soares D (2013) Solid state transformations and equilibrium crystal structures of an Au-Cu alloy with shape memory effect. *Mater Sci Forum* 730–732:859–864
82. Miura S, Okuno H, Ohkubo K, Mohri T (2004) In-situ observation of surface relief formation and disappearance during order-disorder transition of equi-atomic CuAu alloy using laser scanning confocal microscopy. *MRS Online Proc Libr Arch.* <https://doi.org/10.1557/PROC-842-S4.4>
83. Šachl J, Šíma V (2008) A study of order-disorder transformation in CuAu alloy under an external load. *Kovove Mater* 46:277–283
84. Šachl J, Šíma V, Pfeiler W (2004) Reversible and irreversible changes of surface morphology by order-disorder transition in CuAu alloy. *J Alloys Compd* 378(1):274–278
85. Volkov AY, Antonov B, Patselov A (2010) Effect of external force fields on the domain structure of equiatomic CuAu alloy. *Phys Met Metallogr* 110(3):250–259
86. Volkov AY, Kazantsev V (2012) Impact of the initial state on the structure and properties of the ordered CuAu alloy. *Phys Met Metallogr* 113(1):62–71
87. Darling T, Chu F, Migliori A, Thoma D, Lopez M, Lashley J, Lang B, Boerio-Goates J, Woodfiel B (2002) Elastic and thermodynamic properties of the shape-memory alloy AuZn. *Philos Mag B* 82(7):825–837
88. Lashley JC, Ledbetter H, Darling TW, Saxena A, Malinowski A, Hundley MF, Smith JL, Thoma DJ (2006) Free-energy density of the shape-memory alloy AuZn. *Mater Trans* 47(3):587–593
89. Lashley JC, Shapiro SM, Winn BL, Opeil CP, Manley ME, Alatas A, Ratcliff W, Park T, Fisher RA, Mihaila B, Riseborough P, Salje EKH, Smith JL (2008) Observation of a continuous phase transition in a shape-memory alloy. *Phys Rev Lett* 101(13):135703
90. McDonald RD, Goddard PA, Lashley J, Harrison N, Mielke CH, Singleton J, Harima H, Suzuki M-T (2006) High magnetic field studies of the shape memory alloy AuZn. *J Phys Chem Solids* 67(9):2100–2105
91. Svitelskiy O, Suslov A, Singleton J, Lashley JC (2006) Ultrasonic probe of the AuZn fermi surface. In: AIP conference proceedings, AIP, pp 1319–1320

92. Winn B, Shapiro S, Lashley JC, Opeil C, Ratcliff W (2010) Structural phase transition in AuZn alloys. *J Phys: Conf Ser* 251:012027
93. Giordana MF, Muñoz-Vásquez N, Garro-González M, Esquivel M, Zelaya E (2015) Study of the formation of Cu-24at.% Al by reactive milling. *Procedia Mater Sci* 9:262–270
94. Silva R, Machado E, Adorno A, Magdalena A, Carvalho T (2012) Completeness of β -phase decomposition reaction in Cu-Al-Ag alloys. *J Therm Anal Calorim* 109(2):927–931
95. Pascal NS, Giordana M, Napolitano F, Esquivel M, Zelaya E (2017) Thermal stability analysis of Cu-11.8 wt% Al milled samples by TEM and HT-XRD. *Adv Powder Technol* 28(10):2605–2612
96. Adorno A, Guerreiro M, Benedetti AV (2001) Isothermal aging kinetics in the Cu-19 at.% Al alloy. *J Alloys Compd* 315(1–2):150–158
97. Cesari E, Kustov S, Golyandin S, Sapozhnikov K, Van Hulmebeek J (2006) Mobility of point-like defects in Cu-Al martensites. *Mater Sci Eng A* 438:369–373
98. Giordana M, Esquivel M, Zelaya E (2015) A detailed study of phase evolution in Cu-16 at.% Al and Cu-30 at.% Al alloys under different types of mechanical alloying processes. *Adv Powder Technol* 26(2):470–477
99. Giordana MF, Muñoz-Vásquez N, Esquivel M, Zelaya E (2017) Analysis of the Cu-Al milling stages through the microstructure evolution studied by TEM and SEM. *Metallogr Microstruct Anal* 6(2):139–149
100. Graczykowski B, Biskupski P, Mroz B, Mielcarek S, NÓ M, San Juan J (2009) Elastic properties of Cu-Al-Ni shape memory alloys studied by dynamic mechanical analysis. *Smart Mater Struct* 19(1):015010
101. Huang H-Y, Liu J-P, Wang Y, Liu X-F, Xie J-X (2012) Tension-compression asymmetry of stress-induced transformations in martensitic Cu-12 wt.% Al alloys. *Mater Lett* 79:51–54
102. Huang H-Y, Wang Y, Xie J-X (2014) Stress-induced phase transformation characteristics and its effect on the enhanced ductility in continuous columnar-grained polycrystalline Cu-12 wt% Al alloy. *Mater Sci Eng A* 596:103–111
103. Lovey F, Coene W, Van Dyck D, Van Tendeloo G, Van Landuyt J, Amelinckx S (1984) HREM imaging conditions for stacking sequences in 18R martensite of Cu-Al alloys. *Ultramicroscopy* 15(4):345–356
104. Lovey F, Van Tendeloo G, Van Landuyt J, Amelinckx S (1985) High resolution electron microscopy of twin interfaces in 2H and 18R martensites of Cu-Al alloys. *Scr Metall* 19:1223–1228
105. Lovey F, van Tendeloo G, van Landuyt J, Delaey L, Amelinckx S (1984) On the nature of various stacking defects in 18R martensite in Cu-Al alloys A study by high resolution electron microscopy. *Phys Status Solidi (A)* 86:553–564
106. Roulin G, Duval P (1997) Initial stages of ordering obtained by tempering of the disordered martensitic phase of CuAl alloys. *Scr Mater* 37(1):45–51
107. Soliman H, Habib N (2014) Effect of ageing treatment on hardness of Cu-12.5 wt% Al shape memory alloy. *Indian J Phys* 88(8):803–812
108. Tas H, Delaey L, Deruyttere A (1971) Stress induced phase transformations and the shape memory effect in β' Cu-Al martensite. *Scr Metall* 5(12):1117–1124
109. Tas H, Delaey L, Deruyttere A (1973) The self-accommodating character of the β 1 copper-aluminum martensite. *Metall Trans* 4(12):2833–2840
110. Wang Y, Liao B, Liu J, Chen S, Feng Y, Zhang Y, Zhang R (2012) Effects of deep cryogenic treatment on the solid-state phase transformation of Cu-Al alloy in cooling process. *Phase Trans* 85(7):650–657
111. Zhang G, Sauvage X, Wang J, Gao N, Langdon T (2013) Evolution of a martensitic structure in a Cu-Al alloy during processing by high-pressure torsion. *J Mater Sci* 48(13):4613–4619
112. Koyama Y, Ukena T, Nittono O (1982) Phase transformations and shape memory effect in indium lead alloys. *Trans Jpn Inst Met* 23(9):518–529
113. Lubenets S, Natsik V, Pal-Val L, Pal-Val P, Fomenko L (2002) Kinetics of the low-temperature structural transformation in the In-4.3 at.% Cd solid solution. *Low Temp Phys* 28(6):465–474
114. Lubenets SV, Natsik VD, Pal-Val PP, Pal-Val LN, Fomenko LS (1998) Low-temperature structure transformation in In-Cd solid solutions. *Mater Sci Eng A* 256(1):1–7
115. Luo ZP (2012) An overview on the indium-thallium (In-Tl) shape memory alloy nanowires. *Metallogr Microstruct Anal* 1(6):320–326
116. Miura S, Ito M, Nakanishi N (1976) Pseudoelastic behavior and its strain rate dependence in thermoelastic In-Tl martensite. *Scr Metall* 10(1):87–92
117. Pal-Val P, Pal-Val L, Ostapovets A, Vanek P (2008) Low temperature kinetics of In-Cd solid solution decomposition. *Solid State Phenom* 137:35–42
118. Sonu CH, O'Keefe TJ (1994) Characterization of phase transformation behavior in electrolytically produced indium-thallium shape memory alloy films. *Mater Charact* 33(4):311–319
119. Zheng H, Luo Z, Fang D, Phillips FR, Lagoudas DC (2012) Reversible phase transformations in a shape memory alloy In-Tl nanowires observed by in situ transmission electron microscopy. *Mater Lett* 70:109–112
120. Ogawa Y, Ando D, Sutou Y, Somekawa H, Koike J (2017) Martensitic transformation in a β -Type Mg-Sc alloy. *Shape Mem Superelast* 4(1):167–173
121. Ando D, Ogawa Y, Suzuki T, Sutou Y, Koike J (2015) Age-hardening effect by phase transformation of high Sc containing Mg alloy. *Mater Lett* 161:5–8
122. Ogawa Y, Ando D, Sutou Y, Koike J (2016) A lightweight shape-memory magnesium alloy. *Science* 353(6297):368–370
123. Ogawa Y, Ando D, Sutou Y, Koike J (2016) Aging effect of Mg-Sc alloy with α + β two-phase microstructure. *Mater Trans* 57(7):1119–1123
124. Ogawa Y, Ando D, Sutou Y, Koike J (2017) Texture randomization of hexagonal close packed phase through hexagonal close packed/body centered cubic phase transformation in Mg-Sc alloy. *Scr Mater* 128:27–31
125. Ogawa Y, Ando D, Sutou Y, Yoshimi K, Koike J (2016) Determination of α/β phase boundaries and mechanical characterization of Mg-Sc binary alloys. *Mater Sci Eng A* 670:335–341
126. Ogawa Y, Sutou Y, Ando D, Koike J (2018) Aging precipitation kinetics of Mg-Sc alloy with bcc+ hcp two-phase. *J Alloys Compd* 747:854–860
127. Ogawa Y, Sutou Y, Ando D, Koike J, Somekawa H (2019) Ordering of the bcc phase in a Mg-Sc binary alloy by aging treatment. *Metall Mater Trans A* 50(7):3044–3047
128. Yamagishi K, Ogawa Y, Ando D, Sutou Y, Koike J (2019) Room temperature superelasticity in a lightweight shape memory Mg alloy. *Scr Mater* 168:114–118
129. Abhyankar A, D'Santhoshini BA, Kaul S, Nigam A (2008) Effect of site disorder on martensitic transformation in ferromagnetic Ni₅₅Fe₂₀Al₂₅ alloy as inferred from magnetic and magneto-transport measurements. *Adv Mater Res* 52:77–84
130. Chen S, Hsieh S, Lin H, Lin M, Huang J (2008) Electrical discharge machining of a NiAlFe ternary shape memory alloy. *J Alloys Compd* 464(1–2):446–451

131. Jiang C, Sordelet D, Gleeson B (2006) Effects of Pt on the elastic properties of B2 NiAl: a combined first-principles and experimental study. *Acta Mater* 54(9):2361–2369
132. Monastyrsky GE, Ochin P, Odnosum VV, Pasko AY, Kolomytsev VI, Koval Y (2013) Martensitic transformation in Ni-Al-Pt high temperature shape memory alloys. *Mater Sci Forum* 738–739:506–511
133. Ozdemir O, Zeytin S, Bindal C (2010) Characterization of NiAl with cobalt produced by combustion synthesis. *J Alloys Compd* 508(1):216–221
134. Pank D, Nathal M, Koss D (1990) Microstructure and mechanical properties of multiphase NiAl-based alloys. *J Mater Res* 5(5):942–949
135. Russell SM, Law CC, Blackburn MJ (1988) The effect of cobalt on martensitic toughening parameters in NiAl. *MRS Proc* 133:627
136. Valiullin AI, Kositsyna II, Kositsyn SV, Kataeva NV (2008) Stabilization of high-temperature shape memory effect in functional Ni-Al-Co martensitic alloys. *Mater Sci Eng A* 481–482:551–554
137. Kang H-J, Wu S-K, Wu L-M (2010) Martensitic transformation of $\text{Ni}_{64}\text{Al}_{34}\text{Re}_2$ shape memory alloy. *Intermetallics* 18(1):123–128
138. Sun B, Che X, Lin D, Yang G, Zhou Y (1995) The ductility of La-doped rapidly solidified NiAl. *Scr Metall Mater* 33(7):1145–1149
139. Sordelet D, Besser M, Ott R, Zimmerman B, Porter W, Gleeson B (2007) Isothermal nature of martensite formation in Pt-modified β -NiAl alloys. *Acta Mater* 55(7):2433–2441
140. Kang H-J, Wu S-K, Wu L-M (2011) 3R and 14M martensitic transformations in as-rolled and annealed $\text{Ni}_{64}\text{Al}_{34.5}\text{Re}_{1.5}$ shape memory alloy. *J Alloys Compd* 509(5):1619–1625
141. Kaul S, Annie D'Santhoshini B, Abhyankar A, Barquin LF, Henry P (2006) Thermoelastic martensitic transformation in ferromagnetic Ni–Fe–Al alloys: effect of site disorder. *Appl Phys Lett* 89(9):093119
142. Kim HY, Miyazaki S (2004) Martensitic transformation behavior in Ni–Al and Ni–Al–Re melt-spun ribbons. *Scr Mater* 50(2):237–241
143. Kim S, Kim M, Oh M, Hirano T, Wee D (2003) Phase transformation and microstructure of NiAl/Ni₃Al alloys containing Ti. *Scr Mater* 48(4):443–448
144. Chernenko V, Kanth BR, Mukhopadhyay P, Kaul S, Villa E, Gambardella A, Bessegini S (2008) Stress-induced and thermoelastic properties of Ni–Fe–Al melt-spun ribbon. *Appl Phys Lett* 93(14):141904
145. Mukhopadhyay PK, Karmakar M, Rajini Kanth B, Kaul SN (2013) Experimental and theoretical investigations of the stress-induced twinning/detwinning in the martensite phase of a FSMA system. *J Alloys Compd* 577:S119–S122
146. Okumura H, Uemura K (2011) Effects of rotation speed on microstructure and transition temperatures in Ni–Fe–Al melt-spun ribbons. *Intermetallics* 19(12):1996–2001
147. Biffi CA, Agresti F, Casati R, Tuissi A (2015) Ni₃Ta high temperature shape memory alloys: effect of B addition on the martensitic transformation and microstructure. *Mater Today: Proc* 2:S813–S816
148. Firstov G, Koval YN, Van Humbeeck J, Ochin P (2008) Martensitic transformation and shape memory effect in Ni₃Ta: a novel high-temperature shape memory alloy. *Mater Sci Eng A* 481:590–593
149. Kosorukova T, Firstov G, Noël H, Ivanchenko V (2013) Crystal structure changes in the Ni₃Ta intermetallic compound. *Chem Metals Alloys* 6(3–4):196–199
150. Rudajevova A (2010) Study of the thermal properties of a Ni₃Ta shape memory alloy. *Int J Thermophys* 31(2):378–387
151. Rudajevova A, Pospišil J (2010) Shape memory behavior of a Ni₃Ta alloy pre-deformed in compression. *Mater Sci Eng A* 527(12):2900–2905
152. Rudajevova A, Pospišil J (2011) Influence of anisotropy, the latent heat and the thermal history of alloy on martensitic transformation strain in Ni₃Ta single crystal. *J Alloys Compd* 509(18):5500–5505
153. Zhou C, Guo C, Li C, Du Z (2018) Thermodynamic optimization of the Ni–Ta system supported by the key experiments. *Thermochim Acta* 666:135–147
154. Otsuka K, Sawamura T, Shimizu K, Wayman CM (1971) Characteristics of the martensitic transformation in TiNi and the memory effect. *Metall Trans* 2(9):2583–2588
155. Sandrock GD, Hehemann RF (1971) The observation of surface relief during the martensitic transformation in TiNi. *Metallography* 4(5):451–456
156. Otsuka K, Ren X (2005) Physical metallurgy of Ti–Ni-based shape memory alloys. *Prog Mater Sci* 50(5):511–678
157. Frenzel J, George EP, Dlouhy A, Somsen C, Wagner MFX, Eggeler G (2010) Influence of Ni on martensitic phase transformations in NiTi shape memory alloys. *Acta Mater* 58(9):3444–3458
158. Pan CH, Wang YB, Pan HY (2015) Development of dynamically artificial flowers driven by shape memory alloy and pulse width modulation. In: 2015 IEEE international workshop on advanced robotics and its social impacts (ARSO), pp 1–6
159. Active Aliforms, 2023. <http://www.holbrookandcompany.com/>. Accessed 15 Jan 2023
160. <https://www.lamborghini.com/en-en/news/lamborghini-sians-smart-material-system-how-it-works>. Accessed 15 Jan 2023
161. Stoockel D (1990) Shape memory actuators for automotive applications. *Mater Des* 11(6):302–307
162. Jani JM, Leary M, Subic A (2014) Shape memory alloys in automotive applications. *Appl Mech Mater* 663:248–253
163. Chillara VSC, Headings LM, Tsuruta R, Itakura E, Gandhi U, Dapino MJ (2019) Shape memory alloy–actuated prestressed composites with application to morphing automotive fender skirts. *J Intell Mater Syst Struct* 30(3):479–494
164. Ishikawa H, Sutou Y, Omori T, Oikawa K, Ishida K, Yoshikawa A, Umetsu R, Kainuma R (2007) Pd–In–Fe shape memory alloy. *Appl Phys Lett* 90(26):261906
165. Shen Q, Sun W, Wei Z, Liu J (2019) Highly undercooled $\text{Pd}_{59.3}\text{In}_{23.2}\text{Fe}_{17.5}$ alloy: shape memory effect, linear superelasticity and elastocaloric property. *Scr Mater* 160:58–61
166. Shen Q, Zhao D, Sun W, Wei Z, Liu J (2018) Microstructure, martensitic transformation and elastocaloric effect in Pd–In–Fe polycrystalline shape memory alloys. *Intermetallics* 100:27–31
167. Chieda Y, Kanomata T, Umetsu RY, Okada H, Nishihara H, Kimura A, Nagasako M, Kainuma R, Ziebeck KRA (2013) Magnetic phase diagram of Heusler alloys $\text{Pd}_2\text{Mn}_{1+x}\text{Sn}_{1-x}$. *J Alloys Compd* 554:335–339
168. Ito T, Kimura Y, Xu X, Han K, Umetsu RY, Omori T, Kainuma R (2019) Martensitic transformation and shape memory effect in $\text{Pd}_{50}\text{Mn}_{50-x}\text{Ga}_x$ alloys. *J Alloys Compd* 805:379–387
169. Kanomata T, Chieda Y, Okada H, Nishihara H, Kimura A, Nagasako M, Umetsu RY, Kainuma R, Ziebeck KRA (2012) Martensitic transition of Mn-rich Pd–Mn–Sn alloy. *J Alloys Compd* 541:392–395
170. Kanomata T, Endo K, Chieda Y, Sugawara T, Obara K, Shishido T, Matsubayashi K, Uwatoko Y, Nishihara H, Umetsu RY, Nagasako M, Kainuma R (2010) Magnetic properties of Mn-rich Pd_2MnSn Heusler alloys. *J Alloys Compd* 505(1):29–33
171. Xu X, Okada H, Chieda Y, Aizawa N, Takase D, Nishihara H, Sakon T, Han K, Ito T, Adachi Y, Kihara T, Kainuma R, Kanomata T (2019) Magnetoresistance and thermal

- transformation arrest in $Pd_2Mn_{1.4}Sn_{0.6}$ Heusler alloys. *Materials* 12(14):2308
172. Chastaing K, Denquin A, Portier R, Vermaut P (2008) High-temperature shape memory alloys based on the RuNb system. *Mater Sci Eng A* 481:702–706
 173. Denquin A, Chastaing K, Vermaut P, Caillard D, Van Hulbeeck J, Portier R (2009) Shape recovery in RuNb-based high temperature shape memory alloys. In: International conference on martensitic transformations (ICOMAT), Wiley, Hoboken, pp 465–471
 174. Dirand L, Nô M, Chastaing K, Denquin A, San Juan J (2012) Internal friction and dynamic modulus in Ru-50Nb ultra-high temperature shape memory alloys. *Appl Phys Lett* 101(16):161909
 175. Fonda R, Vandermeer R (1997) Crystallography and microstructure of TaRu. *Philos Mag A* 76(1):119–133
 176. Gao X, Zheng Y, Cai W, Zhang S, Zhao L (2004) Microstructure, compression property and shape memory effect of equiautomic TaRu high temperature shape memory alloy. *J Mater Sci Technol* 20(1):97–98
 177. He Z-R, Zhou J-E, Furuya Y (2003) Effect of Ta content on martensitic transformation behavior of RuTa ultrahigh temperature shape memory alloys. *Mater Sci Eng A* 348(1):36–40
 178. Gao X, Cai W, Zheng Y, Zhao L (2006) Martensitic transformation and microstructure in Nb–Ru–Fe shape memory alloys. *Mater Sci Eng A* 438:862–864
 179. Tan C-L, Tian X-H, Cai W (2008) Effect of Fe on martensitic transformation of NbRu high-temperature shape memory alloys: experimental and theoretical study. *Chin Phys Lett* 25(9):3372
 180. Declairieux C, Denquin A, Ochin P, Portier R, Vermaut P (2011) On the potential of $Ti_{50}Au_{50}$ compound as a high temperature shape memory alloy. *Intermetallics* 19(10):1461–1465
 181. Shim H, Tahara M, Inamura T, Goto K, Yamabe-Mitarai Y, Hosoda H (2015) Oxidation behavior of Au-55 mol% Ti high temperature shape memory alloy during heating in Ar-50 vol% O_2 environment. *Mater Trans* 56(4):600–604
 182. Kulinińska A, Wodniecki P (2014) TiPd shape memory alloy studied by PAC method. *Acta Phys Pol A* 4(125):936–939
 183. Matsuda M, Yano S, Nishida M (2011) Morphology and crystallography of martensite plate with long period stacking structure in Ti-Pd shape memory alloy. *Mater Trans* 52(11):2016–2021
 184. Solomon VC, Nishida M (2003) Morphological and crystallographic aspects of C11b-type precipitates nucleated in martensitic and parent phase matrices in Ti-rich Ti-Pd shape memory alloys. *J Phys IV France* 112:1039–1042
 185. Yamamoto T, Morizono Y, Honjyo J, Nishida M (2006) Phase equilibrium and martensitic transformation in near equiautomic TiPd alloys. *Mater Sci Eng A* 438:327–331
 186. Schwartz A, Tanner L (1994) Phase transformations and phase relations in $Ti_{50}Pd_{(50-x)}TM_x$ alloys. *Chem Mater Sci*, Lawrence Livermore National Laboratory, pp 4–6
 187. Schwartz A, Tanner L (1995) Phase transformations and phase relations in the TiPd-TiCr pseudobinary system. 1: Experimental observations. *Scr Metall Mater (United States)* 32(5):675–680
 188. Frankel D, Jiang T, Olson GB (2015) Design of a fatigue resistant Ni-free PdT-base SMA. *Mater Today: Proc* 2:S801–S804
 189. Chikosha S, Chikwanda HK (2013) TiPt HTSMA produced by spark plasma sintering of elemental powders. In: Materials science forum, vol 738. Trans Tech Publ, Switzerland, pp 579–583
 190. Chikwanda HK, Yamabe-Mitarai Y, Chikosha S (2011) Phase analyses of a TtPt alloy synthesized by spark plasma sintering. In: Materials science forum, vol 675. Trans Tech Publ, Switzerland, pp 1143–1146
 191. Mahlatji M, Chikosha S, Chikwanda HK, Stumpf W, Siyasiya C (2014) Thermal properties of amorphous TiPt alloy produced by mechanical alloying. *Adv Mater Res* 1019:372–378
 192. Wadood A, Yamabe-Mitarai Y (2014) TiPt–Co and TiPt–Ru high temperature shape memory alloys. *Mater Sci Eng A* 601:106–110
 193. Wadood A, Takahashi M, Takahashi S, Hosoda H, Yamabe-Mitarai Y (2013) High-temperature mechanical and shape memory properties of TiPt–Zr and TiPt–Ru alloys. *Mater Sci Eng A* 564:34–41
 194. Yamabe-Mitarai Y, Arockiakumar R, Wadood A, Suresh K, Kitashima T, Hara T, Shimojo M, Tasaki W, Takahashi M, Takahashi S (2015) Ti (Pt, Pd, Au) based high temperature shape memory alloys. *Mater Today: Proc* 2:S517–S522
 195. Semenova EL, Petyukh V, Kudryavtsev YV (1995) The effect of cobalt and nickel on transformation in TiRh. *J Alloys Compd* 230(2):115–119
 196. Wu AS, Brown DW, Clausen B, Elmer JW (2017) The influence of impurities on the crystal structure and mechanical properties of additive manufactured U-14at.% Nb. *Scr Mater* 130:59–638
 197. Zhang C, Wang H, Li J, Pang B, Xia Y, Liu Y, Sun G, Zhang X, Fa T, Wang X (2019) The aging-effect-modulated mechanical behavior in U-Nb shape memory alloys through the modified twinning-detwinning process of the α' phase. *Mater Des* 162:94–105
 198. Field R, Brown D, Thoma D (2005) Texture development and deformation mechanisms during uniaxial straining of U-Nb shape-memory alloys. *Philos Mag* 85(13):1441–1457
 199. Tupper CN, Brown DW, Field RD, Sisneros TA, Clausen B (2012) Large strain deformation in uranium 6 wt pct niobium. *Metall Mater Trans A* 43(2):520–530
 200. Carpenter D, Vandermeer R (1982) An X-ray diffraction study of a martensitic transformation in uranium alloys. *Le Journal de Physique Colloques*. <https://doi.org/10.1051/jphyscol:1982458>
 201. Clarke AJ, Field RD, Dickerson PO, McCabe RJ, Swadener JG, Hackenberg R, Thoma D (2009) A microcompression study of shape-memory deformation in U-13 at.% Nb. *Scr Mater* 60(10):890–892
 202. Jackson RJ (1970) Reversible martensitic transformations between transition phases of uranium-base niobium alloys, Dow Chemical Co., Golden, Colo. Rocky Flats Div., pp 1–11
 203. Vandermeer R, Ogle J, Northcutt W (1981) A phenomenological study of the shape memory effect in polycrystalline uranium-niobium alloys. *Metall Trans A* 12(5):733–741
 204. Gao W, Yi X, Sun B, Meng X, Cai W, Zhao L (2017) Microstructural evolution of martensite during deformation in $Zr_{50}Cu_{50}$ shape memory alloy. *Acta Mater* 132:405–415
 205. Meng X, Gao W, Gao Z, Cai W, Zhao L (2014) Substructure and interface of the superstructure martensite in $Zr_{50}Cu_{50}$ high temperature shape memory alloy. *Mater Lett* 117:221–224
 206. Waterstrat RM, Kuentzler R (2003) Structural instability in the B2-type ordered alloys Zr (Ru, Rh) and Zr (Ru, Pd). *J Alloys Compd* 359(1–2):133–138
 207. Filippov V, Yagodin D, Ryltseva A, Estemirova SK, Shunyaev KY (2017) The study of eutectoid decomposition kinetics of $Cu_{50}Zr_{50}$ alloy. *J Therm Anal Calorim* 127(1):773–778
 208. Biffi C, Coduri M, Yoshida H, Soejima Y, Nishida M, Tuissi A (2015) The effect of thermal cycling on the martensitic transformation in equiautomic CuZr shape memory alloy. *J Alloys Compd* 653:591–595
 209. Zheng J, Miao Y, Zhang H, Chen S, Lee D, Arróyave R, Vlassak JJ (2018) Phase transformations in equiautomic CuZr shape memory thin films analyzed by differential nanocalorimetry. *Acta Mater* 159:320–331

210. Semenova OL, Kudryavtsev YV, Petyukh VM, Samelyuk AV (2011) Constitution of ZrCo–ZrIr alloys. *Powder Metall Met Ceram* 49(11):682
211. Nishiura T, Yamamoto T, Hashimoto D, Morizono Y, Nishida M (2006) Martensitic transformation and phase equilibrium in near equiatomic Zr–Pd alloys. *Mater Sci Eng A* 438:852–856
212. Buehler WJ, Wang FE (1968) A summary of recent research on the nitinol alloys and their potential application in ocean engineering. *Ocean Eng* 1(1):105–120
213. Mills SH, Noebe RD, Dellacorte C, Amin-Ahmadi B, Stebner AP (2020) Development of nickel-rich nickel–titanium–hafnium alloys for tribological applications. *Shape Mem Superelast* 6(3):311–322
214. Mills SH, Dellacorte C, Noebe RD, Amin-Ahmadi B, Stebner AP (2021) Rolling contact fatigue deformation mechanisms of nickel-rich nickel–titanium–hafnium alloys. *Acta Mater* 209:116784
215. Arditti SJ, Avedikian SZ, Bernstein BS (1971) Articles with polymeric memory and method of constructing same, Google Patents
216. Schmidt AM (2006) Electromagnetic activation of shape memory polymer networks containing magnetic nanoparticles. *Macromol Rapid Commun* 27(14):1168–1172
217. Chen S, Hu J, Yuen C-W, Chan L (2009) Novel moisture-sensitive shape memory polyurethanes containing pyridine moieties. *Polymer* 50(19):4424–4428
218. Luo X, Mather PT (2009) Preparation and characterization of shape memory elastomeric composites. *Macromolecules* 42:7251–7253
219. Lee H-F, Yu HH (2011) Study of electroactive shape memory polyurethane–carbon nanotube hybrids. *Soft Matter* 8:3801–3807
220. Wu L, Jin C, Sun X (2011) Synthesis, properties, and light-induced shape memory effect of multiblock polyesterurethanes containing biodegradable segments and pendant cinnamamide groups. *Biomacromol* 12(1):235–241
221. Lu XL, Cai W, Gao Z, Tang WJ (2007) Shape memory effects of poly(L-lactide) and its copolymer with poly(ϵ -caprolactone). *Polym Bull* 58(2):381–391
222. Behl M, Razzaq MY, Lendlein A (2010) Multifunctional shape-memory polymers. *Adv Mater* 22(31):3388–3410
223. Xie T (2011) Recent advances in polymer shape memory. *Polymer* 52(22):4985–5000
224. Reyes-Morel PE, Cherng J-S, Chen I-W (1988) Transformation plasticity of CeO₂-stabilized tetragonal zirconia polycrystals: II, pseudoelasticity and shape memory effect. *J Am Ceram Soc* 71(8):648–657
225. Arun D, Chakravarthy P, Arockiakumar R, Santhosh B (2018) Shape memory materials. CRC Press, Boca Raton

Publisher's Note Springer Nature remains neutral with regard to jurisdictional claims in published maps and institutional affiliations.

Springer Nature or its licensor (e.g. a society or other partner) holds exclusive rights to this article under a publishing agreement with the author(s) or other rightsholder(s); author self-archiving of the accepted manuscript version of this article is solely governed by the terms of such publishing agreement and applicable law.